International Journal of Thermal Sciences 226 (2026) 110845

Contents lists available at ScienceDirect

International Journal of Thermal Sciences

journal homepage: www.elsevier.com/locate/ijts

Void fraction profile for subcooled flow boiling through reversing saturation

Francisco J. Collado

Department of Mechanical Engineering, EINA, Universidad de Zaragoza, Maria de Luna 3, Zaragoza, 50018, Spain

ARTICLE INFO

Keywords:
Void fraction profile
Subcooled flow boiling
Mixture enthalpy
Slip ratio
Onset of nuclear boiling (ONB)
Mixture velocity first derivative continuity at saturation
Reversing saturation velocities

ABSTRACT

This work is a continuation of a previous one (F.J. Collado, Phys. Fluids 34, 2022, 123302) where a new model of vapor void fraction was compared against some tests of the void axial profile for upward subcooled flow boiling of water reported by MPI in the eighties. The new void model was based on a new energy balance where heat was divided by the mean vapor-liquid velocity ratio, or slip ratio. The model tried to predict the slip ratio profile, next the mixture enthalpy could be derived from the new heat balance and finally the void fraction was obtained. The mixture enthalpy was based on the classic thermodynamic quality, which includes the void fraction. The slip ratio profile model proposed was dependent on five unknown parameters, although only two new thermo-kinematic equations were suggested then solving two parameters. In this work, the new slip ratio profile model has been simplified to just three parameters and, correspondingly, three new equations have been proposed. First, the continuity of the first derivative of the mixture velocity but here modified by the new slip function. Second, a new equation resulting of the theoretical equilibrium liquid velocity intercept with the reversing vapor velocity from saturation. And third, a new procedure for searching the best location of the onset of nucleate boiling (ONB), which is based on minimizing the absolute error, is suggested. Moreover, thermal approximations to the best ONB found are explored. This simplified void model is favorably checked against the full set (twenty-four) of void fraction profile MPI tests.

1. Introduction

Modeling of subcooled flow boiling is of central interest to a large variety of thermal and hydraulic applications in power and process industries [1,2]. One of the major variables characterizing such liquid-vapor flows is the cross-sectional average of vapor volumetric fraction of vapor bubbles, or void fraction α, which significantly affects heat transfer and pressure drop [1–3] as well as neutron absorption and reactivity in boiling water nuclear reactors [3–5].

However, despite the fact that it has been thoroughly investigated since the 1960's, see Zuber and Findlay [6], and Saha and Zuber [7], recent comparisons of Cai et al., [8] of vertical up-flow axial void fraction datasets with 49 correlations, since 1959 until 2021, conclude that predicting the one-dimensional void fraction profile remains a formidable challenge.

Recently, some research trends are focused on highly resolved 3D flow boiling measurements and the consequent Computational Fluid Dynamics (CFD) simulations [9,10]. Unfortunately, this 3D analysis of bubble dynamics is extremely complex because the detailed analysis of gas-liquid systems involves a wide range of bubble size and shape depending on the flow pattern, which in turn depends on flow conditions like pressure, mass flow rate, geometry, etc. Furthermore, this size range is continuously altered by breakup into the surrounding liquid, and collisions and coalescence between bubbles [9,10]. Therefore, the models used by CFD codes to predict multiphase flows are still incomplete [9,10], and it is recognized that the overall understanding of the mechanisms and the reliability of simulations are yet to be satisfactory [11].

The much simpler standard one-dimensional (1d) bubbly flow models should be based on averaged 1d mass and energy balances for a two-phase flow. However, the steady coexistence of subcooled liquid and saturated vapor bubbles, in addition to the velocity difference between the two phases, confuse standard mass and energy balances.

1.1. 1d standard procedures to calculate void fraction

Due to such non-equilibrium thermal and kinetic complexities in flow boiling, up to three different definitions of the quality, or vapor

E-mail address: fjk@unizar.es.

https://doi.org/10.1016/j.ijthermalsci.2026.110845
Received 19 November 2025; Received in revised form 21 February 2026; Accepted 11 March 2026
Available online 19 March 2026

mass fraction, are considered [3,8]. First, the equilibrium quality x_e, which is derived from the standard heat balance for a flow boiling in a uniformly heated pipe, and it is defined as [3,6–8]

$$x_e = \frac{h_{mixture} - h_F}{\Delta h_{FG}} \tag{1}$$

where $h_{mixture}$, h_F, and Δh_{FG} are the so-called local enthalpy of mixture [3,12], saturated liquid enthalpy, and latent heat of vaporization, respectively.

The expression of $h_{mixture}$ is given by Thom et al., see page 16 in Ref. [12], and Mudawar et al. [8] from the standard heat balance for a flow boiling

$$h_{mixture} = \frac{4q''z}{GD} + h_{Li} = qz + h_{Li} = h_L(z) \tag{2}$$

where h_{Li}, q", G, D and z, are, respectively, the liquid inlet enthalpy, uniform wall heat flux, inlet water mass flux, tube diameter, and axial distance from inlet. By convenience, we have included in Eq. (2) the parameter q, which simply stands for the heat absorbed per unit length of pipe and per unit inlet mass

$$q = \frac{q''(\pi D)}{G(\pi D^2/4)} = \frac{4q''}{GD}. \tag{3}$$

Finally, from the standard heat balance, Eq. (2), the location of the saturation point, where the subcooled liquid reaches saturation, would be

$$h_F = qz_{sat} + h_{Li} \quad \rightarrow z_{sat} = \frac{h_F - h_{Li}}{q}. \tag{4}$$

Before following to analyze the different qualities, the classic simplifications for calculating the thermodynamic properties (in the equilibrium) of the single phases, which make up the non-equilibrium two phase flow, are listed below. These standard assumptions will be strictly followed throughout this work.

1.1.1. Standard assumptions to read equilibrium single phase thermodynamic properties

In this work, for a uniformly heated flow boiling, the basic assumptions for reading equilibrium thermodynamic properties of the liquid and vapor phases in tables will be the same as classic treatments [2,3,6–8,12]. First, all properties along the pipe are read in thermodynamic tables at the inlet pressure p_i. Hence, as first approximation and in order to calculate void fraction, it is assumed that the pressure drop along the channel is small compared with the applied static pressure and that the saturation temperature is constant along the channel [2].

Second, the subcooled liquid enthalpy $h_L(z)$, at some distance z from the inlet, can be calculated from Eqs. (2) and (3) thus, in addition to p_i, the rest of subcooled liquid properties, such as liquid density $\rho_L(z)$, liquid specific volume $v_L(z)$, etc., can be read in thermodynamic tables; while for the saturated liquid properties, with subindex F, only the inlet pressure is needed.

Finally, all steady bubbles in flow boiling are assumed to be saturated vapor at inlet pressure, so the rest of saturated vapor properties, e.g., vapor enthalpy h_G, vapor density ρ_G, vapor specific volume v_G, etc., can be found in tables.

1.1.2. Standard calculation of the void fraction from flow quality

With regards to the equilibrium quality, Eq. (1), a main problem, clearly recognized [2,3,6–8,12], is that we cannot derive the vapor content from this standard heat balance, Eqs. (1)–(3), because x_e is negative along the subcooled region until reaching saturation.

Therefore, a second quality is usually defined: the so-called flow quality, or mass dryness fraction, x_d. x_d is classically considered the true flow fraction of vapor [3,6–8], and is defined as the vapor-total mass flow rate ratio,

$$x_d = \frac{W_G}{W_G + W_L} = \frac{\rho_G u_G \alpha A}{\rho_G u_G \alpha A + \rho_L u_L (1-\alpha) A}, \tag{5}$$

where W_G, W_L, A, u_G, and u_L are, respectively, the mass flow rate of saturated vapor, mass flow rate of subcooled liquid, cross-sectional area of the pipe, cross-sectional average velocity of saturated vapor, and cross-sectional average subcooled liquid velocity.

Obviously, it is not possible to derive the dryness fraction, Eq. (5), from the classic heat balance, Eq. (2). In fact, this one of the major drawbacks of standard 1d flow boiling i.e., the lack of a heat balance that directly includes the vapor content of the flow boiling through the subcooled zone. To avoid this important difficulty, there have been proposed [8] several appropriate (empirical) $x_d(z)$ relations in function of the equilibrium quality, $x_e(z)$, plus the equilibrium quality just at the point of net vapor generation (NVG), or onset of significant void (OSV), $x_{e,OSV}$.

Remark that the subcooled flow boiling actually starts at the so-called onset of nucleate boiling (ONB) [1–3,6–8,13,14], where the first little bubbles appear on the heated surface despite the bulk liquid remains subcooled. This first subcooled zone, with very low void fraction values, ranges from ONB ($\alpha \sim 0$) until around $\alpha \leq 2-4$ % [15] and it is usually neglected in standard void fraction models [8]. So, standard models consider that α practically commences later, at the OSV, from where the void fraction increases rapidly due to the progressive bulk liquid heating. More details can be found in Refs. [6–8,13,14].

Logically, to calculate x_d some correlation for $x_{e,OSV}$ is also needed. That is why the ability to calculate the onset of significant void accurately is currently considered one of the most important elements in predicting the axial void fraction profile in the subcooled flow boiling region [3,6–8,13–15]. Following Mudawar et al. [8], the most used empirical correlation for $x_d(z)$ is the Saha and Zuber correlation [7] including exponential expressions in such a way that $x_d(z_{OSV}) = 0$, in coherence with the above commented simplification for the practical origin of α.

Finally, the standard void fraction predictive procedures try to relate α with the flow quality x_d. The most relevant categories are the slip ratio and drift flux models [8]. The slip ratio procedures [8] are based in some combination of the standard void fraction and mass dryness fraction that includes the slip ratio S, or vapor-liquid velocity ratio, given by $S = u_G/u_L$.

The drift flux void fraction model, proposed by Zuber and Findlay [6], is a variation of the slip model substituting the slip ratio by two new parameters i.e., a distribution parameter, C_0, related to the non-uniformity of the flow profile, and the so-called drift velocity, v_{gj}, or the local relative velocity between the phases. Indeed, the concept of drift velocity was proposed to consider kinematic non-equilibrium between two-phases [5]. Differences among the various drift flux models lie in the choice of expressions for C_0 and v_{gj}, which are different for different flow patterns and obtained empirically or theoretically [8].

Notice that the assessment of void fraction models performed by Mudawar et al. see Table 3 in Ref. [8] only covers until 2012 (with the exception of their own proposal). Recently, Hibiki [16] has conducted a state-of-the art review on one-dimensional drift-flux correlations for various flow channel geometries and flow orientations, which extends until 2018.

Finally, as the above drift-flux two parameters are critical in the one-dimensional two-fluid model used in current nuclear thermal-hydraulic system analysis codes [16], some quite recent advances on the drift-flux model are briefly commented.

1.1.3. Recent advances in the drift-flux void fraction modeling

First, most existing drift-flux correlations for C_0 and v_{gj} were developed for specific flow regimes and patterns [8,17] breaking down the full range of void fraction values i.e., from 0 to 1. Indeed, drift-flux

correlations valid for the full-range of the void fraction were limited and rather complex [16,17]. Quite recently, Hibiki et al. [17] developed a simple full-range drift-flux correlation applicable for upward two-phase flows in vertical pipes, which was validated against compiled experimental database.

Second, point out that the extensive void fraction model review of Mudawar and coworkers is strictly limited to one channel geometry and one flow orientation i.e., subcooled boiling vertical up-flow in a circular tube [8]. However, there are many other important channel geometries and orientations e.g., upward two-phase flow in vertical rectangular and annulus channels, and vertical sub-channel of the rod bundle, horizontal two-phase flow in a circular channel, etc., which have been recently addressed through the drift-flux model in Refs. [4,5,16–18].

And third, the usual evaluation of different void fraction predictive tools is based on comparing directly the whole consolidated data point set e.g., 1118 void points in Ref. [8], with the whole predicted data points of the previous models and correlations. Therefore, the one-dimensional steady measured void profiles, which are the original source of data point sets, are lost. Furthermore, as it has been remarked above, the first subcooled region previous to the OSV, with very low void fraction values, is neglected in the consolidated data set.

However, very recently, Hibiki and Dong [19] have presented a new model that not only predicts actual profiles of the void fraction profile in upward boiling flows in vertical round tubes but also covers the pre-OSV region. The new void profile model was fairly compared with measured void fraction profiles, which conform an experimental database containing 788 data points from seven independent sources. The source with higher number of data (323 points) is the void profile set measured at the Moscow Power Institute (MPI) in the eighties by γ-ray attenuation for water at medium-high pressure and subcooling by Bartolomei et al. [20]. In this work, this data source will be also used later to assess the new void model proposed here.

1.2. New 1d steady energy balance for flow boiling. Void fraction based on thermodynamic mixture enthalpy

As it has been advanced above, the main issue about standard one-dimensional void fraction models [4–8,13–19] is attempting to connect α with the flow quality x_d because this quality is neither directly related with the void fraction nor with the standard heat balance. Therefore, standard void fraction models need two stages of empirical correlations to relate α with flow quality. First, an empirical relation [8,21] between the equilibrium quality x_e and x_d, and second, correlations for C_0 and v_{gj}, based again on empirical correlations [4,5,8,16–19] between the previously flow quality empirically found and the desired void fraction.

Indeed, the standard heat balance is merely an equilibrium balance assuming that before the saturation point there is only subcooled liquid. The reality, confirmed by thousands of measurements, is that there is a co-existence of subcooled liquid and saturated vapor in thermal and kinetic non-equilibrium along the subcooling zone.

The core proposal of this work is to test against data new one-dimensional steady non-equilibrium mass and heat balances for subcooled flow boiling, proposed by the author elsewhere [22,23]. These new balances should be the core of new predictive tools for void fraction profiles, which would supply more accurate calculations and with less empiricism than standard models [8,19].

In order to overcome the current difficulties for calculating void fraction [8,19], the starting proposal of the author about 1d flow boiling modeling [22,23] was to work with the well-known 'static' or thermodynamic quality, x, which is the third vapor mass fraction considered in standard analysis [3]. x is classically defined [3] as

$$x\left[\frac{kg\ vapor}{kg\ mixture}\right]=\frac{\alpha\rho_G\left[\frac{kg\ vapor}{m^3\ mixture}\right]}{\rho_m\left[\frac{kg\ mixture}{m^3\ mixture}\right]}, \tag{6}$$

where ρ_m, the standard mixture density [1–3,6–8], and its inverse, the specific mixture volume v_m, are, respectively,

$$\rho_m=\rho_G\alpha+\rho_L(1-\alpha);\qquad v_m=\frac{1}{\rho_m}=xv_G+(1-x)v_L. \tag{7}$$

This was first suggested by Bilicki and Michaeliades [24], who noted that if we were able to measure α by γ-ray its corresponding actual mass fraction, following Thermodynamics, should be x, not x_d. Then, any new flow boiling energy balance should be based on the thermodynamic mixture enthalpy h_m, which now is defined in function of the thermodynamic quality x,

$$h_m=xh_G+(1-x)h_L=h_m(\alpha). \tag{8}$$

Highlight the strong connection between h_m and void fraction α through x. Then, if we were able to predict h_m, we could easily find α from Eqs. (6)–(8). Indeed, the above three equations are the core of the new void fraction model. Hence, we should search for a new heat balance between thermodynamic mixture enthalpy increments Δh_m and the absorbed heat per unit mass i.e., qz.

For bulk flow boiling, the author already analyzed in Ref. [22] the accurate 286 tests of the outlet void fraction α_o measured with γ-ray attenuation by Knights [25] during the Cambridge project for vertical and horizontal saturated water flow boiling. The pressure and mass flux ranged from 1.72 MPa to 14.48 MPa and from 561 to 1833 kg/m^{2}s, respectively. As main result of this analysis [22], it was found that the classic or 'flow' slip ratio S_{flow} would close the new thermodynamic heat balance based on h_m

$$S_{flow}=\frac{u_{G,o}}{u_{F,o}}=\frac{x_{d,o}\rho_F(1-\alpha_o)}{(1-x_{d,o})\rho_G\alpha_o}\sim\frac{qz_o}{\Delta h_m(\alpha_o)}=\frac{qz_o}{h_m(\alpha_o)-h_F}, \tag{9}$$

where z_o is the full length of the tube test, $u_{G,o}$ and $u_{F,o}$ are the vapor and saturated liquid outlet velocities, respectively whereas $x_{d,o}$ is the outlet flow quality derived from the standard heat balance i.e., $x_{d,o}=qz_o/\Delta h_{FG}$. Moreover, $h_m(\alpha_o)$ means that this thermodynamic mixture enthalpy is calculated with the thermodynamic quality, which includes the measured outlet void fraction, through Eqs. (6)–(8). Remark that, in Eq. (9), the standard relation between S_{flow}, flow quality, densities and void fraction is obtained from the classic liquid and vapor mass flow rates formulated in Eq. (5). Also note that, in these tests [25], water was entered at saturated state (subindex F) in the test tube.

For subcooled flow boiling, the actual behavior of $h_m(z)$ against qz was already checked in Ref. [23] using the above commented void fraction profile data measured at the MPI [20]. As it happened with bulk flow boiling analysis in Ref. [22], the plot of $h_m(z)$ showed significant discrepancies with $qz+h_{Li}$ [23]. Then, based on the foregoing results [22] for saturated flow boiling, it was again suggested that such discrepancy could be corrected including the slip ratio. Therefore, the new heat balance for subcooled flow boiling would be

$$S_{exp}(z)=\frac{u_G(z)}{u_L(z)}\sim\frac{qz}{\Delta h_m(\alpha_{exp})}, \tag{10}$$

where $\Delta h_m(\alpha_{exp})$ means thermodynamic mixture enthalpy increments calculated from the experimental void data profiles $\alpha_{exp}(z)$ following Eqs. (6)–(8). So, from Eq. (10), it was possible to derive an 'experimental' slip ratio profile $S_{exp}(z)$.

The above derived 'experimental' slip profile exhibited two clearly distinct zones [23]. The first zone, along subcooled flow boiling, here denoted $S_1(z)$, showed an approximated linear decay from $S_1(z_{OSV})=1$ until saturation $S_1(z_{sat})=S_{1,sat}$, with $S_{1,sat}$ slightly less than one for all

the tests reported in Ref. [20]. Notice that, following standard analysis [8], it was assumed that flow boiling practically started at the OSV. Just at the saturation point, the beginning of the second zone, the slip ratio experiments a strong discontinuity and its value jumps from $S_{1,sat}$ to S_2 that is clearly greater than one. Given the satisfactory simulation results in Ref. [23], S_2 could be considered practically constant along bulk flow.

In conclusion, only three unknown parameters namely, z_{OSV}, $S_{1,sat}$ and S_2 could define the slip ratio profile. For each one of the 24 tests reported by MPI, these three parameters where varied in order to find the best fitting of the corresponding slip ratio profile [23]. One of the main results was to check that if we were able to reproduce the slip ratio profile, the thermodynamic mixture enthalpy could be acceptably derived from Eq. (10). Then, the void fraction profile could be fairly calculated from Eqs. (6)–(8).

A possible justification for including the slip ratio in Eq. (10), suggested elsewhere [22,23], could be that the times scales of the phases must be different each other because we are considering that the liquid velocity is different from that of vapor but in the same control volume length. If the times scales were not different, the velocities should be the same. This time scale difference should be regarded in the heat balance formulation.

In Eq. (10), q is the heat flux q" divided by the inlet mass flux of water G, see Eq. (3). If we assume that q" enters into the control volume through vapor bubbles (vapor time scale) that condense in the subcooled water, Eq. (10) would mean that S could act as a time scale conversion factor between the vapor phase (q"-condensing bubbles) and the liquid phase (G).

1.3. New 1d steady mass balance for flow boiling

Now, if we include the slip ratio in the 'flow' quality x_d, as a time scale conversion factor between the vapor and liquid phases, we obtain the thermodynamic quality x

$$x_d = \frac{W_G}{W_G + W_L} \rightarrow \frac{W_G/S}{W_G/S + W_L} = \frac{\rho_G u_L \alpha A}{\rho_G u_L \alpha A + \rho_L u_L (1-\alpha) A} = \frac{\rho_G u_L \alpha A}{u_L \rho_m A} = x. \tag{11}$$

In Eq. (11), the vapor time scale variables are divided by the slip ratio before to combine them with the liquid time scale variables.

By correspondence with the 'flow' quality concept [3] i.e., vapor mass flow rate divided by the total mass flow rate, Eq. (11) would suggest a new 1d steady mass balance for flow boiling, coherent with the above new heat balance,

$$W_{L,i} = \frac{W_G}{S} + W_L = \rho_G u_L \alpha A + \rho_L u_L (1-\alpha) A = \rho_m u_L A \rightarrow G = \frac{W_{L,i}}{A} = \rho_{Li} u_{Li} = \frac{u_L}{v_m}, \tag{12}$$

where $W_{L,i}$ ρ_{Li} and u_{Li} are the inlet mass flow rate of liquid, inlet liquid density and inlet liquid velocity, respectively. As in Eq. (11), the vapor mass flow rate W_G is divided by the vapor-liquid velocities ratio to convert its vapor time scale to that of the liquid one, which is taken as reference. As a theoretical confirmation of this new 1d steady mass balance for flow boiling, the author has presented elsewhere [26] a new general 3D mass conservation equation for a two-phase flow strictly applying the Reynolds transport theorem, which has resulted coherent with the above Eq. (12).

Moreover, Eq. (12) has been confirmed through void fraction data. Recently [27], it has been checked the continuity of the first derivative of the mixture specific volume v_m just at saturation, where v_m was calculated with the MPI void data [20]. Point out that, due to Eq. (12), the first derivative continuity of v_m implies the first derivative continuity of u_L, since $u_L = Gv_m$, with G a constant. Moreover, classic kinematics [28] assumes continuity of motion equations and their derivatives. Therefore, the first derivative continuity of v_m supports both Eq. (12) and that u_L be considered as the representative mixture velocity.

On the other hand, some thermo-kinetic equations to model the slip ratio profile were recently proposed in Ref. [27]. In this model, at difference from the simpler treatment in Ref. [23] and by coherence with classic treatments, the subcooled region of the flow boiling was divided in two regions i.e., the first one started just at the onset of nucleate boiling (ONB), in order to include even the few steady bubbles between the ONB and the OSV, and the second one begun and the onset of significant void (OSV). However, this meant to work with five parameters. In particular, the location of ONB z_{ONB}, the location of OSV z_{OSV}, the vapor void fraction at OSV α_{OSV}, $S_{1,sat}$, and S_2. Therefore, five thermo-kinetic equations should be found.

As a first approach, the three first parameters of the slip profile model i.e., z_{ONB}, z_{OSV}, and α_{OSV}, were merely varied [27] to fit the predicted void profile to data. Finally, two new thermo-kinematic equations completed the five parameters model. The first one was the continuity of the first derivative of v_m just at saturation commented above. The second thermo-kinematic equation merely linked the ONB and S_2 through the vapor velocity profile along bulk flow boiling. S_2 was considered constant as in Ref. [23].

Solving the non-linear two thermo-kinematic equations system with only two unknowns i.e., $S_{1,sat}$, and S_2, the slip ratio profile model was complete. Inserting this slip model in Eq. (10), the thermodynamic mixture enthalpy is derived then the void profile is found from Eqs. (6)–(8). The agreement of the calculated void profiles and the experimental ones was acceptable. However, as we have noticed above, the three first parameters were fitted to void profiles data by trial and error based on visual inspection. Besides, the model was only compared [27] against 8 out of the 24 tests in Ref. [20].

1.4. Objectives of the present work

The work presented here exhibits several advantages over the previous five-parameter slip ratio model [27]. First, it has been simplified to only three ones namely, z_{ONB}, $S_{1,sat}$, and S_2. This simplification would be supported by the acceptable results found in Ref. [23], which were only based on three parameters. Second, we present two new thermo-kinetic equations, which include the above three parameters. Third, instead of the simple trial and error procedure used in Ref. [27], the accurate measurement of the void fraction profiles taken by MPI [20] could serve as a 'third equation' if we looked, for each test, the best z_{ONB}. The best ONB point for each profile will be found plotting the absolute error simulations in function of the z_{ONB} used and looking for the minimum. Fourth, some thermal approximations to the best ONB found are also explored. And fifth, at difference from the previous work [27], here the void calculations are compared against the full twenty-four measured axial void profiles reported by MPI [20].

Clearly, if this simplified slip ratio model worked acceptably, the void fraction prediction would be highly simplified. Therefore, the main objective of this work is to check the ability of this new three-parameter model to predict void fraction profiles in subcooled flow boiling of water under conditions of industrial interest.

The structure of this work is as follows. Section 2 briefly reviews, for one of the tests, void data reduction for calculating the 'experimental' thermodynamic mixture enthalpy necessary to derive the 'experimental' slip ratio profile from the new heat balances. Section 3 proposes simple slip ratio profile models that should fit the 'experimental 'slip ratio profile. The simple slip model only depends on (z_{ONB}, $S_{1,sat}$, S_2), so three new thermo-kinematic equations are needed. Section 4 shows the first equation i.e., the first derivative continuity of the mixture specific volume but now for the simpler slip model. Section 5 develops the second equation based on intersections of a theoretical 'equilibrium' velocity with backward extensions of the bulk vapor velocity profiles. Section 6 explains how the void profile data are used, in combination with the two new thermo-kinetic equations, for searching the best ONB point looking for the minimum absolute error. Section 7 explores a thermal approximation to the best ONB previously found, which is based on classic

studies from Griffith, Clark and Rohsenow [29]. After solving the non-linear equations system, section 8 compares the calculated void profiles with void data [20] and discusses the new model. Finally, section 9 gives some conclusions.

2. Void data reduction, new heat balance and 'experimental' slip ratio

2.1. Operating variables of the MPI tests

Table 1 gathers the measured operating variables of the tests [20] and some results. Whereas the first column identifies the test, the next four variables are the operating conditions. In particular, inlet pressure p_i, mass flux G, uniform heat flux q", and inlet subcooling $\Delta T_{sub,i}$, which range from 3.01 to 14.68 MPa, from 405 to 2123 kg/m^{2}s, from 0.42 to 2.21 MW/m^2, and from 11.2 to 140.4 K, respectively. The next two ones i.e., the inlet subcooled liquid velocity u_{Li} and the saturation point z_{sat}, are easily calculated from inlet data. The slope of the saturated vapor velocity u'_{G2}, which is relevant for the simulation, follows. The rest are the second equation proposed and the 'best' location of the ONB and its thermal approximation, which will be explained later.

The upward channels used [20] were made of 12 $\times$ 10^{-3} m ID commercial tubes and 2 $\times$ 10^{-3} m of wall thickness, with heated lengths from 0.8 to 1.5 m. For all the tests performed, maximum relative errors did not exceed 0.01 for pressure, 0.02 for mass velocity, 0.03 for heat flux density and 1 K for temperature. For the true volumetric steam content α, determined by γ-radiation, the maximum absolute error did not exceed $\pm$ 0.04.

Fig. 1 shows the experimental void fraction profile for test 1-1 in Table 1. The measured void values (circles) were originally reported as a function of x_e [20]. The relation between x_e and z is shown in Eqs. (1)–(3). The calculated void profile (bold line) through the new slip ratio profile model is explained later.

2.2. 'Experimental' thermodynamic mixture enthalpy profile $h_m(z)$

In Fig. 2, the 'experimental' h_m(z) profile is plotted (circles) following Eq. (8) that includes the thermodynamic quality x. In turn, x is derived from Eqs. (6) and (7), using the void fraction data (circles) from Fig. 1. Thermodynamic properties have followed standard assumptions, see subsection 1.1.1.

The discrepancy between $h_m(z)$ and the classic heat balance for flow boiling $qz + h_{Li}$, Eq. (2), represented by the fine blue line, is quite clear. The bold line is the calculated mixture enthalpy explained later. The strong discontinuity of the enthalpy slope at saturation was already justified in Ref. [27].

In this work, the slip ratio profile model has been reduced to only three parameters (z_{ONB}, $S_{1,sat}$,S_2). Then, the flow along the tube has been divided into three zones. First, a single liquid phase flow zone from the inlet of the uniformly heated tube until the onset of nucleate boiling (ONB), where S is set to 1 by coherence between Eqs. (2) and (10). Next, two simple boiling zones follow i.e., subcooled flow boiling from ONB until saturation (z_{sat}), called zone 1, and bulk flow boiling from saturation onwards, zone 2.

In the following, the 'experimental' S profile for test 1-1 is displayed inserting the above 'experimental' mixture enthalpy in the new heat balance, Eq. (10). Thus, detailed expressions of the new heat balance are previously needed.

2.3. Simplified heat balance along subcooled flow boiling. Slip ratio S_1

The new simplified heat balance proposed along subcooled flow, which extends from ONB, which is a key unknown of the model, until saturation, is

$$h_{m1}(z) = \frac{q}{S_1(z)}(z - z_{ONB}) + h_{L,ONB} \;\rightarrow\; \{S_1(z)\}_{exp} \approx \frac{q(z - z_{ONB})}{\{h_{m1}(z)\}_{exp} - h_{L,ONB}} \tag{13}$$

where subindex 1 stand for the subcooled zone, subindex exp means that such variable has been calculated through measured void data, and $h_{L,ONB}$ is the subcooled liquid enthalpy at the ONB point, z_{ONB}, ($h_{L,ONB} = qz_{ONB} + h_{L,i}$). It is assumed that there is only liquid at ONB [1–3].

Eq. (13) justifies the discrepancies between the 'experimental' mixture enthalpy, black circles in Fig. 2, and the standard heat balance, fine blue line, inserting $S_1(z)$. It not presupposes any assumption about how $S_1(z)$ should be. In the second part of Eq. (13), $\{S_1(z)\}_{exp}$ is derived from the new heat balance including the 'experimental' thermodynamic mixture enthalpy-void data from Fig. 2.

The last mixture enthalpy value for the subcooled zone will be that of saturation

$$h_{m,sat} = \frac{q}{S_1(z_{sat})}(z_{sat} - z_{ONB}) + h_{L,ONB}, \tag{14}$$

where $S_{1,sat}$, a major (unknown) parameter of the model, is the saturation value of S_1 along the subcooled flow. Logically, to preserve enthalpy continuity, this enthalpy should also be the first value of the following bulk flow boiling or zone 2.

2.4. Simplified heat balance along saturated (bulk) flow boiling. Slip ratio S_2

The heat balance along bulk flow, which extends from saturation onwards, would be given by

$$h_{m2}(z) = \frac{q}{S_2(z)}(z - z_{sat}) + h_{m,sat} \;\rightarrow\; \{S_2(z)\}_{exp} \approx \frac{q(z - z_{sat})}{\{h_{m2}(z)\}_{exp} - h_{m,sat}} \tag{15}$$

Again, in Eq. (15), we do not know a priori how $S_2(z)$ should be.

2.5. 'Experimental' slip ratio from void data

Finally, Fig. 3 shows the 'experimental' slip ratio profile S_{exp} (blue points), which is worked out inserting 'experimental' mixture enthalpies, see Fig. 2, in the second part of Eqs. (13) and (15). Notice two differences from Ref. [27]: now $S_1(z)$ starts at ONB and this simple slip has only one discontinuity just at saturation.

The S_{exp} behavior is practically the same as that in Ref. [23] then, in this work, the suggested fittings for S_{exp} are quite similar. Along the subcooling zone, there would be a slight linear decay from the ONB, S_1 (z_{ONB}) = 1, until saturation, S_1 (z_{sat}) = $S_{1,sat}$. Although a quadratic function will be also explored.

After the ONB point, there is a steady, although rather slow, growth of the steam content in the flow boiling. In Fig. 2, can be seen that, as the new thermodynamic mixture enthalpy (circles) does include vapor, it should be greater than local enthalpy of mixture (fine blue line). Coherently, the experimentally derived S_1 takes values lower than 1 in order to $h_m > qz + h_{Li}$ along subcooling flow.

Just at saturation, there is a strong discontinuity and the 'experimental' slip ratio jumps from S_1 values definitely lower than 1 to S_2 values clearly greater than 1. Along bulk flow, S_2 presents a saw-tooth profile but, in spite of this irregular profile, the previous assumption [23,27] of the constancy of S_2 (other major unknown) along saturation has also supplied in this work acceptable predictions not only for S_{exp}, see Fig. 3, but also for the void fraction, see the bulk flow zone in Fig. 1. Some reasons of this slip ratio discontinuity, which is only suffered by the vapor velocity, have been already suggested in Ref. [27]. On the other hand, the liquid phase is considered the continuous one.

Table 1
Operating conditions of Bartolomei et al. tests [20]. Slip ratio parameters, 2nd equation and mean absolute error.

Test	p_i (MPa)	G (kg/m^{2}s)	q" (MW/m^2)	$\Delta T_{sub,i}$ (K)	z_{sat} (m)	u_{Li} (m/s)	u'_{G2} (s^{-1})	$z_{onb} = f \cdot z_{therm}$	Best z_{ONB} (m)	$S_{1,sat}$	S_2	z-intercept	2nd Equation	#Eqs. Text	$\frac{\sum \lvert \Delta \alpha \rvert}{n}$ (%)
1-1 L	6,89	985	1,13	93,9	1,17	1,12	6,61	1,12* $z_{1/2}$	0,608	0,879	2835	z_G	$u_{L2}(z_G) = u_{eq1}(z_G)$	(29) & (34)	0,48
1-2 L	6,78	1071	1,13	91,8	1,25	1,22	6,70	0,96* $z_{1/2}$	0,58	0,848	2198	z_G	$u_{L2}(z_G) = u_{eq1}(z_G)$	(29) & (34)	0,85
1-3 L	6,84	961	1,13	91,4	1,11	1,10	6,65	1,09* $z_{1/2}$	0,535	0,860	2416	z_G	$u_{L2}(z_G) = u_{eq1}(z_G)$	(29) & (34)	0,63
1-4 L	6,84	995	1,15	91,4	1,13	1,13	6,77	1,10* $z_{1/2}$	0,555	0,865	2525	z_G	$u_{L2}(z_G) = u_{eq1}(z_G)$	(29) & (34)	0,58
2a-1 Q	6,81	998	0,44	36,1	1,24	1,24	2,60	0,89* $z_{1/2}$	0,55	0,880	2031	$z_0 = 0$	$u_{G2,sat} = z_{sat} * u'_{G2}$		0,73
2a-2 L	6,89	965	0,78	64,9	1,18	1,14	4,56	0,97* $z_{1/2}$	0,51	0,846	2226	z_G	$u_{L2}(z_G) = u_{Li}$	(29) & (35)	0,55
2a-4 Q	6,74	988	1,70	140,4	1,13	1,07	10,13	0,99*$z_{1/2}$	0,49	0,897	2303	z_G	$u_{L2}(z_G) = u_{eq1}(z_G)$	(29) & (34)	0,59
2a-5 Q	7,01	996	1,98	125,1	0,88	1,09	11,40	0,77* $z_{1/2}$	0,20	0,920	2946		$z_0 = z_{1/3} - (u_{Li}/u'_{G2})$		0,76
3a-1 L	6,89	405	0,79	136,9	0,98	0,44	4,62	1,16* $z_{1/2}$	0,515	0,859	2359	z_G	$u_{L2}(z_G) = u_{eq1}(z_G)$	(29) & (34)	1,06
3a-3 Q	6,89	1467	0,77	38,9	1,12	1,81	4,50	$z_{2/3}$	0,235	0,848	1523	z_G	$u_{G2}(z_G) = u_{eq1}(z_G) \approx u_{Li}$	(29) & (36)	1,29
3a-4 Q	6,79	2024	0,78	36,9	1,45	2,51	4,62	$z_{2/3}$	0,506	0,851	1570	z_G	$u_{G2}(z_G) = u_{eq1}(z_G) \approx u_{Li}$	(29) & (36)	0,32
3b-1 Q	11,02	503	0,99	97,4	0,76	0,59	3,80	$z_{2/3}$	0,037	0,899	2045	z_G	$u_{L2}(z_G) = u_{Li}$	(29) & (35)	1,62
3b-2 Q	10,81	966	1,13	87,9	1,17	1,16	4,42	0,93* $z_{2/3}$	0,29	0,881	1789	z_{eq0}	$u_{L2}(z_{eq0}) = u_{Li}$	(33) & (37)	0,82
3b-3 Q	10,81	1554	1,16	26,9	0,63	2,10	4,54	0,87*$z_{2/3}$	−0,34	0,802	1503	z_G	$u_{G2}(z_G) = u_{eq1}(z_G) \approx u_{Li}$	(29) & (36)	0,84
3b-4 L	10,84	1959	1,13	27,1	0,82	2,65	4,41	0,78*$z_{1/3}$	0,24	0,856	1509	z_{Li}	$u_{G2}(z_{Li}) = u_{Li}$	(38)	0,84
2b-1 L	14,79	1878	0,42	11,2	1,12	2,89	1,23	1,31* $z_{1/2}$	0,305	0,904	2529		$u_{G1,sat} = u_{Li}$	(39)	0,62
2b-2 Q	14,74	1847	0,77	15,9	0,83	2,78	2,27	1,15* $z_{1/3}$	0,275	0,856	1359		$u_{G1,sat} = u_{Li}$	(39)	1,04
2b-3 Q	14,75	2123	1,13	31	1,16	3,02	3,32	$z_{2/3} = 0,042$	0,0	0,884	1628	z_{eq0}	$u_{G2}(z_{eq0}) = u_{Li}$	(33) & (40)	0,52
2b-4 Q	14,7	2014	1,72	68,7	1,43	2,59	5,07	0,94* $z_{1/2}$	0,540	0,873	1489	z_{eq0}	$u_{G2}(z_{eq0}) = u_{Li}$	(33) & (40)	0,85
2b-5 Q	14,99	2012	2,21	52,3	0,89	2,70	6,40	0,84*$z_{1/2}$	0,065	0,847	1214	$z_{1/2}$	$u_{G2}(z_{1/2}) = 0$		0,58
4a-1 Q	3,01	990	0,98	62,2	0,85	1,10	11,88	1,16* $z_{1/2}$	0,28	0,919	3315		$z_0 = z_{1/3} - (u_{Li}/u'_{G2})$		0,98
4a-2 Q	4,41	994	0,9	66,4	1,02	1,13	7,80	$z_{2/3} = 0,214$	0,21	0,910	2851	z_L	$u_{L2}(z_L) = u_{eq1}(z_L)$	(30) & (41)	0,81
4a-5 L	14,68	1000	1,13	80,6	1,23	1,26	3,34	0,98*$z_{1/2}$	0,49	0,817	1401	z_{eq0}	$u_{G2}(z_{eq0}) = u_{eq,g}(z_{eq0})$	(33) & (42)	1,33
4b-1 L	6,81	2037	1,13	53,1	1,42	2,45	6,67	$z_{1/3} = 0,933$	0,928	0,785	1479	z_{eq0}	$u_{G2}(z_{eq0}) = u_{eq,g}(z_{eq0})$	(33) & (42)	0,44

See subsection 5.1 for definition of z_G, z_L,z_{eq0}, z_{Li} and velocities. Definition of $z_{2/3}$, $z_{1/2}$ and $z_{1/3}$ in section 7.

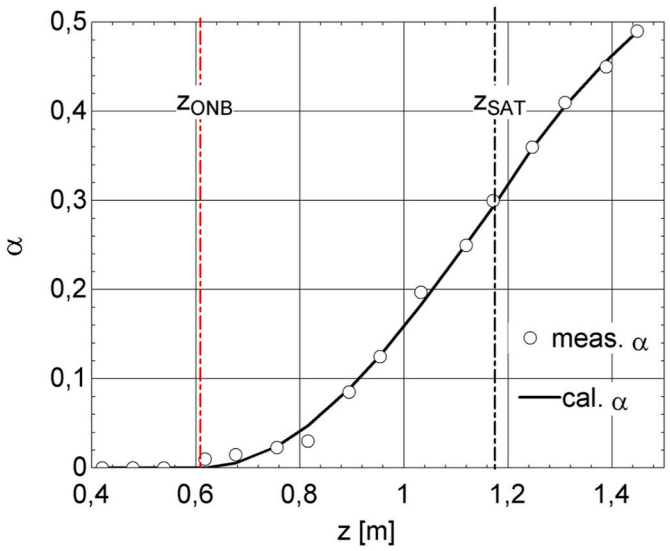

Fig. 1. Void fraction (α) profile for test 1-1 L. Table 1.

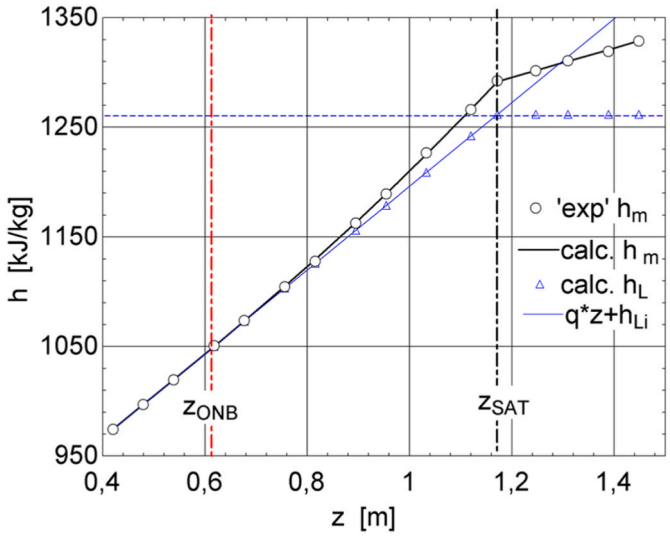

Fig. 2. Mixture enthalpy (h_m) profile for test 1-1 L. Table 1.

2.6. New simple procedure to calculate the void fraction profile

Remark that the new procedure to predict the void fraction profiles suggested in this work simply consists in calculating the mixture enthalpy profiles along subcooling, first part of Eq. (13), and also along bulk flow boiling, first part of Eq. (15) with Eq. (14). Remember that, in this work, the mixture enthalpy is based on the thermodynamic enthalpy. Thus, through Eqs. (6)–(8), the α values can be readily worked out.

As can be seen in the new proposed heat balance, Eqs. (13-(15), besides the operating conditions of the tests, see Table 1, the value of z_{ONB}, some expressions for $S_1(z)$ along subcooling and the value of S_2 are needed to calculate such enthalpy profiles. As we will see next, the chosen expressions for $S_1(z)$ are only function of z_{sat}, see Eq. (4), and two unknowns: z_{ONB} and $S_{1,sat}$. In conclusion, as we have advanced above, the main objective of this work is to search for and solve a non-linear three equations system, which contained the three basic unknowns $(z_{ONB}, S_{1,sat}, S_2)$.

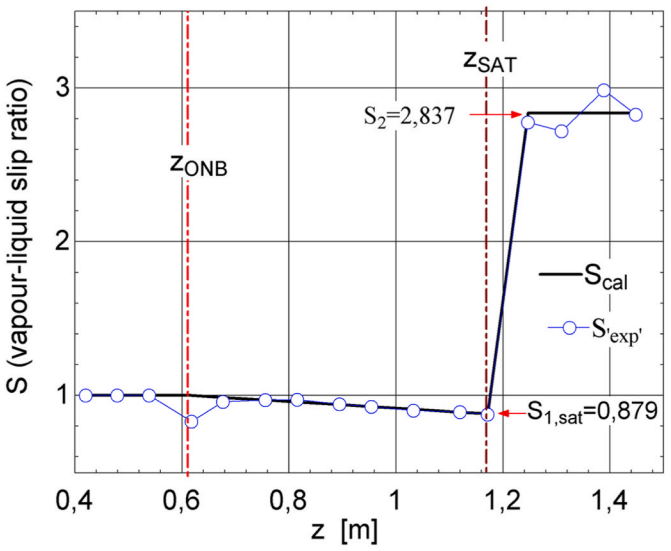

Fig. 3. Slip ratio (S) profile for test 1-1 L in Table 1.

3. A three parameters slip ratio profile model

3.1. Two new functions for $S_1(z)$

Depending on operating conditions, there have been found two options to fit the 'experimental' slip ratio $S_1(z)$ along the subcooled zone: a linear function, different from Ref. [27] because here the boiling starting point is the ONB, and a brand-new quadratic function. In Table 1, the tests that respond to the linear slip function are marked with a L whereas those that have been modeled with the quadratic one appears with a Q. As we have advanced above, both $S_1(z)$ functions are function of z_{sat} and two unknowns i.e., z_{ONB} and $S_{1,sat}$.

3.1.1. New linear function (L) for $S_1(z)$

Based on the $\{S_1(z)\}_{exp}$ found, a new linear slip function suggested for zone 1 and its derivative (a constant) would be

$$\{S_1(z)\}_{cal} = 1 + \frac{(S_{1,sat}-1)}{(z_{sat}-z_{ONB})}(z-z_{ONB}) \rightarrow S_1' = \frac{(S_{1,sat}-1)}{(z_{sat}-z_{ONB})}. \tag{16}$$

3.1.2. New quadratic function (Q) for $S_1(z)$

The new quadratic slip function for zone 1 and its derivative (a linear function) are

$$\{S_1(z)\}_{cal} = 1 + \frac{(S_{1,sat}-1)}{(z_{sat}-z_{ONB})^2}(z-z_{ONB})^2 \rightarrow S_1'(z) = \frac{2(S_{1,sat}-1)}{(z_{sat}-z_{ONB})^2}(z-z_{ONB}). \tag{17}$$

By convenience, both for the quadratic and the linear slip functions, the value of the slip ratio just at saturation coming from subcooling (zone 1) is defined as

$$S_{1,sat} = \frac{u_{G1,sat}}{u_{L,sat}}, \tag{18}$$

where $u_{G1,sat}$ is the vapor velocity just at saturation coming from subcooling and $u_{L,sat}$ is the liquid velocity just at saturation.

3.2. Constancy of the slip ratio along saturation, S_2

By completeness, the above commented constancy of S_2 along bulk boiling [23,27] is also stated:

$$\{S_2\}_{cal} = constant \rightarrow S_2 = \frac{u_{G2}(z)}{u_{L2}(z)} \rightarrow S_2 = \frac{u_{G2,sat}}{u_{L,sat}}. \quad (19)$$

where $u_{G2,sat}$ is the vapor velocity just at saturation but coming from saturation. These two distinct values of the vapor velocity just at saturation i.e., $u_{G1,sat}$ and $u_{G2,sat}$, are due to the strong discontinuity experimented by the vapor at this point, see Figs. 2 and 3.

3.3. Relation of $S_{1,sat}$ and $u_{L,sat}$ at saturation. Unknowns of the non-linear equations system

The continuous liquid velocity at saturation $u_{L,sat}$, which appears in Eqs. (18) and (19), is tightly related with the mixture specific volume, or its inverse the mixture density, through the new mass balance, Eq. (12)

$$G = \rho_m u_L = \frac{u_L}{v_m} = \rho_{m,sat} u_{L,sat}. \quad (20)$$

Thus, as the liquid and vapor have already reached thermal equilibrium at saturation, we can read $\rho_{m,sat}$ in thermodynamic tables with p_i and $h_{m,sat}$, last one including $S_{1,sat}$, see Eq. (14). These relations of $u_{L,sat}$ with $S_{1,sat}$, Eq. (20), $u_{G1,sat}$, Eq. (18), and $u_{G2,sat}$, Eq. (19), would be used later in developing the second thermo-kinematic equation, which is based on velocities relations. Therefore, these key saturated velocities are included in the equations system.

4. First equation: continuity of the liquid velocity first derivative at saturation

The first equation suggested relating z_{ONB}, $S_{1,sat}$, and S_2 is again the continuity of the first derivative of the specific volume (or the velocity) of the mixture just at saturation proposed elsewhere [27]. As we have advanced, Eq. (12), this velocity would be the liquid one [23,27]. However, the slip profiles suggested in this work are different from that used in Ref. [27] so the first derivative continuity equation respect to z (channel axial coordinate) have to be calculated again. The first thermo-kinematic equation will be given by

$$v'_{m1}(z_{sat}) = v'_{m2}(z_{sat}), \quad (21)$$

where the prime symbol denotes the first derivative respect to z, subscript 1 means tending to z_{sat} from subcooling and subscript 2 denotes tending to saturation point from the bulk zone. The derivation from subcooling (zone 1) has two options: the new linear $S_1(z)$, Eq. (16), or the new quadratic slip, Eq. (17). Besides, $v'_{m2}(z_{sat})$ can be derived readily from the bulk heat balance, Eq. (15), with S_2 considered constant along the saturation zone.

4.1. $\{v'_{m1}(z_{sat})\}_L$ for the new linear $S_1(z)$ function (L)

v_m, Eq. (7), is formulated for the subcooled boiling (zone 1) and derived with respect to z

$$v'_{m1} = [x(v_G - v_L) + v_L]' = x'(v_G - v_L) - xv'_L + v'_L. \quad (22)$$

Then, x' is worked out from h_m, Eq. (8), which is related with z through the new simple subcooling heat balance, Eq. (13). In this case, the new linear $S_1(z)$ in Eq. (13) is Eq. (16). Finally, the derivative is evaluated at saturation

$$\{v'_{m1}(z_{sat})\}_L = \underbrace{q\frac{(v_G - v_F)}{(h_G - h_F)}\left(\frac{1}{(S_{1,sat})^2} - 1 + x_{sat}\right)}_{x'_1(z_{sat})(v_G - v_F)} + (1 - x_{sat})\underbrace{\frac{\beta(p_i, T_{sat})v_F q}{c_{p,L}(p_i, T_{sat})}}_{v'_L}. \quad (23)$$

The full derivation details of $x'_1(z_{sat})$, which are similar to those in Ref. [27], are shown in Appendix A1. The second addend in Eq. (23), is the derivative of the liquid specific volume, v'_L, evaluated at saturation, which was already derived in Ref. [27]. In particular, β is the volumetric coefficient of thermal expansion at constant pressure, and $c_{p,L}$ is the liquid specific heat at constant pressure.

4.2. $\{v'_{m1}(z_{sat})\}_Q$ for the new quadratic $S_1(z)$ function (Q)

For the new quadratic slip function for zone 1, Eq. (17), the full details of the first derivative, at saturation, of the mixture specific volume coming from subcooling are shown in Appendix A2. The result is

$$\{v'_{m1}(z_{sat})\}_Q = \underbrace{q\frac{(v_G - v_F)}{(h_G - h_F)}\left(\frac{2 - S_{1,sat}}{(S_{1,sat})^2} - 1 + x_{sat}\right)}_{x'_1(z_{sat})(v_G - v_F)} + (1 - x_{sat})\underbrace{\frac{\beta(p_i, T_{sat})v_F q}{c_{p,L}(p_i, T_{sat})}}_{v'_L} \quad (24)$$

4.3. $v'_{m2}(z_{sat})$ for constant S_2

To calculate $v'_{m2}(z_{sat})$, v_m, Eq. (7), is formulated for the bulk zone and then derived

$$v_{m2}(z) = x_2 v_G + (1 - x_2)v_F \rightarrow v'_{m2}(z) = x'_2(v_G - v_F). \quad (25)$$

x'_2, the first derivative of x along the bulk zone (zone 2) is readily found obtaining x_2 from the mixture enthalpy definition, Eq. (8), calculating the mixture enthalpy derivation from the heat balance in the bulk zone, Eq. (15), and finally substituting into Eq. (25),

$$x_2 = \frac{h_m - h_F}{h_G - h_F} \rightarrow x'_2 = \frac{h'_m}{h_G - h_F} = \frac{q}{S_2(h_G - h_F)} \rightarrow v'_{m2}(z) = \frac{q}{S_2}\frac{(v_G - v_F)}{(h_G - h_F)}, \quad (26)$$

where the first derivative of the mixture specific volume along saturation results to be a constant.

5. Second equation: reversing vapor and liquid velocities from saturation to subcooling

In [27], the second thermo-kinematic equation suggested arose from the observation of velocity profiles and their intersections. We were searching for any relation between the unknown key saturated velocities, which take part in the slip ratio definitions, see Eqs. (18)–(20), and some values that were known or could be easily calculated. Here, we have followed the same procedure although including direct and reverse velocities of the liquid, vapor and a new 'equilibrium' velocity.

Following the 1d steady model proposed, Fig. 4, for test 1-1 L in Table 1, shows the direct kinetic profiles, with uniform heating of the tube, of the liquid velocity profile (continuous blue line), Eq. (12), and the vapor one (red line with a strong discontinuity at saturation), Eq. (10). Along subcooling, zone 1, both profiles are curved lines but, as we will see below, along saturation (zone 2) they are straight lines denoted as $u_{L2}(z)$ and $u_{G2}(z)$ for liquid and vapor, respectively. These profiles are calculated after achieving a fair void profile simulation. The circles simply indicate the location of void measurements.

Besides, the locations of the key saturated velocities that make up the slip ratios, see Eqs. (18)–(20), are also indicated in Fig. 4. $u_{L,sat}$ is the liquid velocity just at saturation. On the other hand, due to the discontinuity commented in section 3, the vapor velocity at saturation may take two possible values i.e., $u_{G1,sat}$ coming to saturation from the subcooling zone and $u_{G2,sat}$ coming from the bulk zone. The inlet liquid velocity u_{Li} (dashed horizontal black line) is also included.

At difference from Ref. [27], a new 'equilibrium' velocity profile (green line with a discontinuity of the first derivative at saturation) has been added, Fig. 4. As we will see later, along subcooling, its kinetic profile is a curved line called $u_{eq1}(z)$ but, along saturation its profile is a straight line denoted as $u_{eq2}(z)$. This theoretical 'equilibrium' velocity is

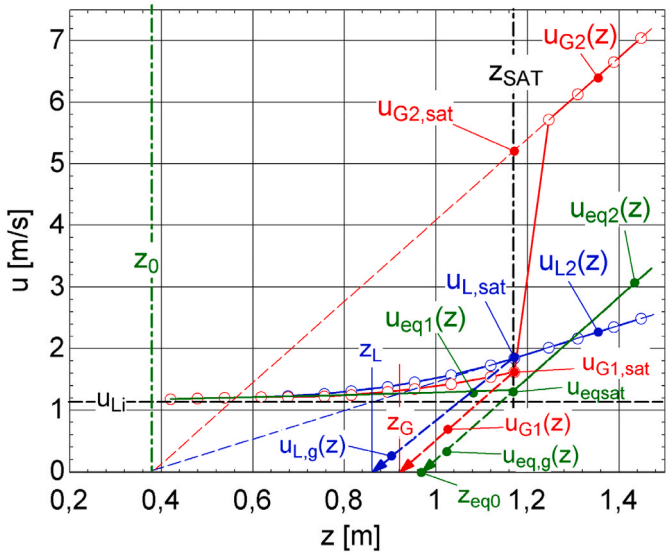

Fig. 4. Liquid (blue), vapor (red) and equilibrium (green) direct and reverse (dashed) kinetic profiles Test 1-1 L. Table 1. (For interpretation of the references to colour in this figure legend, the reader is referred to the Web version of this article.)

based on the standard heat balance, Eqs. (1)–(3), assuming equilibrium conditions throughout the uniformly heated pipe. The 'equilibrium' velocity is easy to calculate and does not contain any of the main unknowns, see Eqs. (18)–(20).

The second kinematic equation suggested here would arise from assuming a theoretical reversion of the uniform heating provoking that liquid and vapor came back from the saturated zone to the subcooled one. As main assumption, which would be based on the uniform heat applied, all the backward processes from saturation would be represented by (dashed) straight lines, see Fig. 4. Previously, the liquid, vapor and equilibrium velocities profiles are analyzed following the proposed model.

5.1. Direct and reverse saturated liquid and vapor velocities

First, the slope of the direct saturated liquid velocity, $u_{L2}(z)$, straight blue line from saturation onwards in Fig. 4, is calculated. From the new mass balance, Eqs. (12) and (20), and the above Eq. (26), it can be readily checked that it is a straight line

$$u_{L2}(z) = Gv_{m2}(z) \rightarrow u'_{L2} = Gv'_{m2} = G\frac{q}{S_2}\frac{(v_G - v_F)}{(h_G - h_F)} = constant. \tag{27}$$

In Fig. 4, the fine dashed blue line would be its theoretical backward extension (reversing the process) from the saturated liquid velocity $u_{L,sat}$ towards the subcooling zone. Taking into account the uniform heating, it has been assumed that this reverse process from saturation to subcooling is linear, with the same slope as the direct one, Eq. (27). The z-intercept of the backward saturated liquid velocity is denoted by z_0.

The straight red line from saturation onwards is the saturated vapor velocity $u_{G2}(z)$, Fig. 4. Considering the slip ratio definition along bulk flow, Eq. (19), the above Eq. (27) and the assumed constancy of S_2, it is easy to show that its slope is a constant too,

$$u_{G2}(z) = S_2 u_{L2}(z) \rightarrow u'_{G2} = S_2 u'_{L2} = Gq\frac{(v_G - v_F)}{(h_G - h_F)} = \frac{4}{D}q''\frac{(v_G - v_F)}{(h_G - h_F)} = constant, \tag{28}$$

where q has been substituted by the heat flux q" following Eq. (3). Again, the fine dashed red line is the backward extension (reversing the process) from the saturated vapor velocity $u_{G2,sat}$ towards the subcooling zone. As before, it has been assumed that this backward extension along subcooling is also a straight line with the same slope as the forward one. The z-intercept of the reverse saturated vapor velocity from $u_{G2,sat}$ is also z_0.

Due to the strong discontinuity of the vapor velocity at saturation, which has two different values at the same position, the reverse process from saturated vapor towards subcooling could also start from the other saturated vapor velocity, $u_{G1,sat}$, near the saturated liquid, see Fig. 4. It is also assumed that this backward extension is a straight line (bold dashed red line) with the same slope u'_{G2} as before. This backward saturated velocity is denoted by $u_{G1}(z)$. A relevant point is z_G i.e., the z-intercept of $u_{G1}(z)$,

$$u_{G1}(z) = u_{G1,sat} - u'_{G2}(z_{sat} - z) \rightarrow \quad 0 = u_{G1,sat} - u'_{G2}(z_{sat} - z_G) \tag{29}$$

From preliminary analysis, it has been found that the reverse process from saturated vapor towards subcooling could also cross at the saturated liquid velocity, $u_{L,sat}$, see bold dashed blue line in Fig. 4. Again, this backward extension is assumed to be a straight line with the same slope u'_{G2}. This backward saturated vapor velocity is denoted by $u_{L,g}(z)$. A relevant point is z_L i.e., the z-intercept of $u_{L,g}(z)$,

$$u_{L,g}(z) = u_{L,sat} - u'_{G2}(z_{sat} - z) \rightarrow \quad 0 = u_{L,sat} - u'_{G2}(z_{sat} - z_L) \tag{30}$$

Besides the saturated vapor and liquid velocities and their backward extensions, the 'equilibrium' liquid velocity, $u_{eq}(z)$, which would follow the standard heat balance, Eq. (2), may participate in the second thermo-kinetic equation, bold green line in Fig. 4.

5.2. Direct and reverse 'equilibrium' velocity

It is assumed that the flow in a theoretical equilibrium along subcooling would be only liquid because if there were also vapor, it would be in thermal and kinematic non-equilibrium with the subcooled liquid. From saturation onwards, it is assumed that both liquid and vapor are saturated and in thermal and kinematic equilibrium each other. Thus, there is a very strong change of slope of the equilibrium velocity in reaching saturation. From continuity, the equilibrium velocity is defined as the product of the inlet liquid mass flux G and the corresponding equilibrium specific volume along subcooling (1) and bulk (2) zones, respectively

$$u_{eq1}(z) = Gv_L(z); \quad u_{eq2}(z) = Gv_{eq2}(z) = G\{(x_{eq}v_G + (1 - x_{eq})v_F\}, \tag{31}$$

where u_{eq1} is the equilibrium velocity of the subcooled liquid along subcooling (only liquid), and u_{eq2} is the velocity of the saturated liquid-vapor mixture along bulk flow, both in thermal and kinetic equilibrium; x_{eq} has been already worked out in Eqs. (1) and (2), and its derivative is immediate $x'_{eq} = q/(h_G - h_F)$.

Hence, along saturation, the slope of the equilibrium velocity would also be a constant,

$$u'_{eq2}(z) = Gv'_{eq2}(z) = Gx'_{eq}(v_G - v_F) = \frac{4}{D}q''\frac{(v_G - v_F)}{(h_G - h_F)} \rightarrow \quad u'_{eq2} = u'_{G2}, \tag{32}$$

which results equal to that of $u_{G2}(z)$, Eq. (28). The bold dashed green line, Fig. 4, would be the reverse process from saturated vapor towards subcooling now crossing saturation at $u_{eq,sat}$, and is called $u_{eq,g}(z)$. Notice that the backward process from saturation to subcooling of the $u_{eq2}(z)$ velocity (in equilibrium) would be $u_{eq1}(z)$, which is in equilibrium too.

The z-intercept of the backward velocity $u_{eq,g}(z)$ is denoted by z_{eq0}, which can be readily found. First, the equilibrium velocity at saturation is given by $u_{eq,sat} = Gv_F$, then z_{eq0} is merely the intersection of a straight line, origin $u_{eq,sat}$ and slope u'_{eq2}, with the z axis

$$u_{eq,g}(z) = u_{eq,sat} - u'_{G2}(z_{sat} - z) \rightarrow \quad 0 = Gv_F - u'_{G2}(z_{sat} - z_{eq0}). \tag{33}$$

In the following, the 2nd thermo-kinematic equation found for each test

is explained. We search linear relations between the unknowns, Eqs. (18)–(20), and some known values. Advance that besides the commented z-intercepts, changes of pressure, heat flux and inlet velocity are relevant. Also note that the slope u'_{G2} depends on pressure through saturation properties, calculated from EES (Engineering Equation Solver) [30], see Table 2. Thus, u'_{G2}, see Eq. (28), gathers pressure, heat flux and diameter, the last one constant in Ref. [20]. Table 1 shows the z-intercept used in the 2nd equation, the 2nd equation found and the corresponding equation numbers in the text.

5.3. Second equation for water at 7 MPa

5.3.1. Set 1 tests (G ~ 1000, q" ~ 1,13). Test 2a-4 Q (G ~ 1000, q" ~ 1,70). Test 3a-1 L (G ~ 405, q" ~ 0,79)

First, the test 1-1 L, at 6,89 MPa, with a mass flux G near 1000 kg/m^{2}s ($u_{Li} = 1,12\ m/s$) and a heat flux q'' of 1,13 MW/m^2, see Table 1, is analyzed in Fig. 4. It is assumed that the reverse process from saturated vapor towards subcooling would start from the lower saturated vapor velocity, $u_{G1,sat}$. Then, the backwards extension (bold dashed red line) of the vapor velocity is $u_{G1}(z)$ with slope u'_{G2}, see Eq. (28), and z-intercept z_G defined in Eq. (29).

There are two unknowns in Eq. (29) namely, $u_{G1,sat}$ and z_G. Then, a second equation is needed. From inspection of Fig. 4-test 1-1 L, it has been found that z_G is also the axial coordinate of the intersection of the backward saturated liquid velocity $u_{L2}(z)$ (fine dashed blue line) with the subcooled equilibrium velocity, $u_{eq1}(z)$, last one defined in Eq. (31),

$$u_{L2}(z_G) = u_{eq1}(z_G) \rightarrow u_{L,sat} - \left(u'_{G2} / S_2\right)(z_{sat} - z_G) = Gv_L(z_G). \quad (34)$$

Eq. (34) would be the second thermo-kinetic equation for test 1-1 L, while Eq. (29) defines the z-intercept z_G included in Eq. (34), see Table 1. This 2nd equation has supplied suitable simulations of the void fraction profile for a total of six out of twenty-four tests [20]. Namely, the four first tests in Table 1 (set 1), with similar conditions i.e., G ~ 1000 kg/m^{2}s and q" ~ 1,13 MW/m^2, in addition to test 2a-4 Q with G ~ 1000 kg/m^{2}s and q" = 1,70 MW/m^2, and finally test 3a-1 L with G ~ 400 kg/m^{2}s and q" = 0,79 MW/m^2. Next, the 7 MPa tests that do not verify Eq. (29) and/or Eq. (34) are analyzed.

5.3.2. Rest of tests 2a and 3a

All tests of the set 2a, see Table 1, have a similar velocity, around 1,1 m/s ($G \sim 1000\ kg/m^2s$), but increasing heat flux. Test 2a-1 Q fulfills neither Eq. (29) nor Eq. (34). It has a rather low heat flux $q'' = 0.44\ MW/m^2$, then, see Eq. (28), the lowest slope, $u'_{G2} = 2,60\ m^{-1}$, of the 7 MPa tests. Hence, the z-intercept of $u_{G1}(z)$ is rather low too compared with the intersections of the backward $u_{L2}(z)$ with $u_{eq1}(z)$ or u_{Li} , which occur at much higher z-coordinates. However, z_0, the z-intercept of $u_{G2}(z)$ backwards, is zero, so supplying a very simple second equation: $u_{G2,sat} = z_{sat} \cdot u'_{G2}$, see Table 1.

Test 2a-2 L with $q'' = 0.78\ MW/m^2$, Fig. 5, has a low slope $u'_{G2} = 4,56\ m^{-1}$, so z_G is not large enough for the backward $u_{L2}(z)$ to intersect with $u_{eq1}(z)$ at z_G, and Eq. (34) is not verified. However, this reverse $u_{L2}(z)$ does intersect with u_{Li} at z_G since u_{Li} is lower than $u_{eq1}(z)$. The second equation for this test is quite simple,

Table 2
Specific volume-enthalpy evaporation ratio for water at different pressures [30] in Table 1.

Pressure (MPa)	$\frac{(v_G - v_F)}{(h_G - h_F)}$ (m^3/MJ)
3	0,03636
4,4	0,026
6,89	0,01754
10,81	0,01173
14,79	0,008795

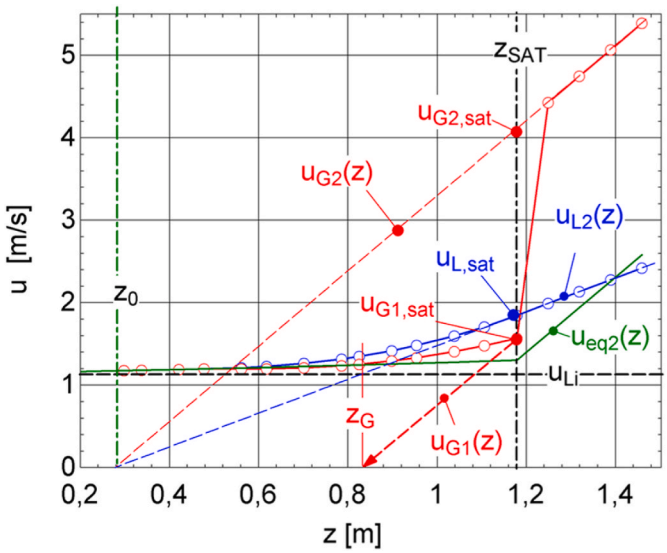

Fig. 5. Thermo-kinetics of test 2a-2 L. Table 1.

Comparing test 2a-2 L with test 3a-1 L ($q'' = 0.79\ MW/m^2$) in Fig. 6, notice that 3a-1 L does fulfill Eqs. (29)-(34) in spite of having a u'_{G2} as low as test 2a-2L i.e., $4,62\ m^{-1}$ vs. $4,56\ m^{-1}$. The reason could be that the 3a-1 L inlet velocity is much lower than that of test 2a-2 L i.e., 0,44 m/s vs. 1,14 m/s. Logically, this low inlet velocity also means a lower equilibrium velocity $u_{eq}(z)$ thus giving option to the backward $u_{L2}(z)$ to intersect $u_{eq1}(z)$ at z_G.

Test 2a-3 does not appear in Table 1 because it is indeed test 1-1 L, with $q'' = 1.13\ MW/m^2$ and $u'_{G2} = 6,65\ m^{-1}$. Logically, for the same pressure, increasing the heat flux implies a higher saturated vapor slope.

Finally, test 2a-5 Q has the highest heat flux of set 2a, $q'' = 1.98\ MW/m^2$, so the highest $u'_{G2} = 11,40\ m^{-1}$. Clearly, z_G is much larger than before but z_L is also high for the reversing $u_{L2}(z)$ to intersect with either u_{Li} or $u_{eq1}(z)$. The 2nd equation found for this test, see Table 1, is rather different from above although similar to that proposed in Ref. [22] but now using $z_{1/3}$, which will be defined in the next section.

On the other hand, all the tests of set 3a, see Table 1, have the same

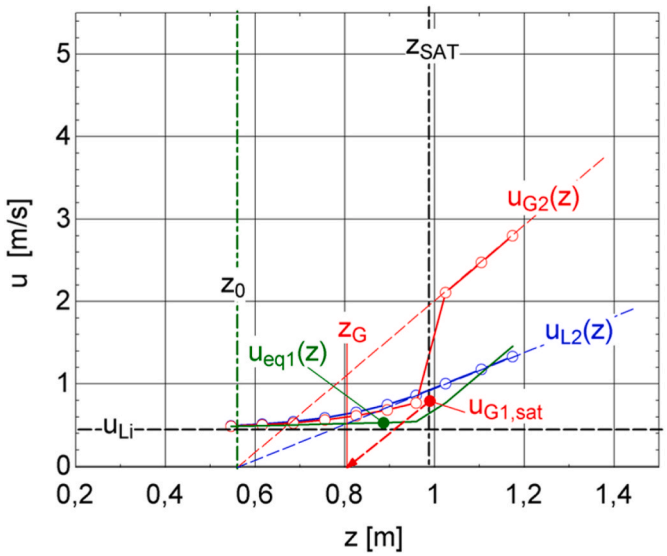

Fig. 6. Thermo-kinetics of test 3a-1 L. Table 1.

heat flux $q'' \sim 0,78\ MW/m^2$ but increasing mass flux. The first test, 3a-1 L, has been already commented above, see Fig. 6. The following would be 3a-2 but indeed it is 2a-2 L, already analyzed, see Fig. 5.

Finally, test 3a-4 Q, see Fig. 7, satisfies neither Eq. (29) nor Eq. (34) in spite of having exactly the same slope as test 3a-1 L. This is due to 3a-4 Q has a much higher mass flux (2024 kg/m^{2}s) than the 3a-1 L one (405 kg/m^{2}s). This means a much higher inlet velocity and also a higher equilibrium velocity. Thus, backward $u_{L2}(z)$ can intersect neither the equilibrium velocity nor the inlet one at z_G, which now is much lower than such intersections. However, the reversing saturated vapor velocity $u_{G2}(z)$ does be able to intersect the equilibrium velocity $u_{eq1}(z)$ at z_G. As we will see later, with high mass fluxes, it is the backward saturated vapor velocity that intersects to the equilibrium velocity or even the inlet one, given the closeness of these last two velocities. Test 3a-3 Q has the same behavior as 3a-4 Q one.

For these two last tests, the second equation would be

$$u_{G2}(z_G) = u_{G2,sat} - u'_{G2}(z_{sat} - z_G) = u_{eq1}(z_G) \approx u_{Li}. \ \rightarrow \ u_{G2,sat} = u_{G1,sat} + u_{Li}, \tag{36}$$

where the simplified Eq. (36), which is the second part of Eq. (36), is derived assuming that the backward saturated vapor velocity intersected the inlet velocity at z_G, see Fig. 7.

5.4. Second equation for water at 11 MPa-Tests 3b

All the tests at 11 MPa, set 3b in Table 1, have nearly the same heat flux $q'' \sim 1,13\ MW/m^2$ but increasing mass flux. Moreover, their saturated vapor slope u'_{G2} are lower than those at 7 MPa with similar heat fluxes due to a higher pressure, Table 2. Test 3b-1 Q, see Fig. 8, has a lower u'_{G2} (3,80 m^{-1}) than test 2a-2 L (u'_{G2} = 4,56 m^{-1}). However, the 2nd equation for 3b-1 Q is the same as that of 2a-2 L, which could be justified again by the lower inlet velocity of 3b-1 Q.

Fig. 9 shows the kinetic profiles for test 3b-2 Q. It has a slightly higher u'_{G2} $(4,42\ m^{-1})$ than test 3b-1 Q, see Table 1, but also an inlet velocity about twice greater. Then, its backward $u_{L2}(z)$ in test 3b-2 Q can intersect neither $u_{eq1}(z)$ nor u_{Li} at z_G, and much less at z_L. Indeed, the reverse $u_{L2}(z)$ intersects u_{Li} at z_{eq0}, see Eq. (33), instead of z_G,

$$u_{L,sat} - \left(u'_{G2} \,/\, S_2\right)\left(z_{sat} - z_{eq0}\right) = u_{L,i}. \tag{37}$$

For test 3b-3 Q, with $G = 1554\ kg/m^2s$, not only the slope u'_{G2} but also the inlet mass flux are very similar to those of tests 3a-3 Q and 3a-4 Q. The second equation is again Eq. (36), which is the same as the above tests. Therefore, it would seem that tests with the same u'_{G2} and similar mass flux would also verify the same second equation.

Finally, see Fig. 10, for test 3b-4 L with $G = 1959\ kg/m^2s$, and $q'' = 1,13\ MW/m^2$, the slope of the saturated vapor velocity is $u'_{G2} = 4,41\ m^{-1}$. Besides this u'_{G2} is slightly lower than those of tests 3a-3 Q, 3a-4 Q and 3b-3 Q, its inlet velocity is the highest out of the four ones. In this case, the second equation suggested is

$$u_{Li} = u_{G2,sat} - u'_{G2}(z_{sat} - z_{Li}) \rightarrow \ u_{G2,sat} = 2u_{Li}, \tag{38}$$

where z_{Li} is the z-intercept of a linear velocity with origin at u_{Li} and saturation, and slope u'_{G2}. As before, a simpler second equation for this test 3b-4 L has been derived from inspection of Fig. 10. This could be justified because lower the saturated vapor velocity slope and higher the inlet velocity, more to the left the abscissa of the intersection of the backward $u_{G2}(z)$ with u_{Li} goes. Thus, the above new intercept should originate more to the right.

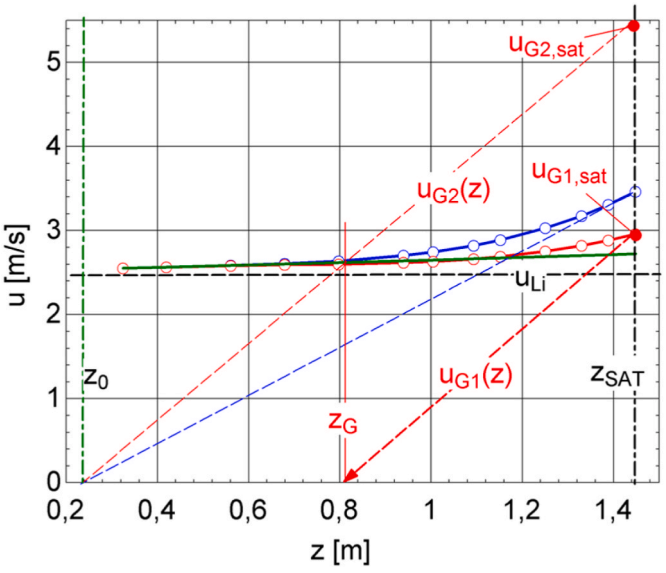

Fig. 7. Thermo-kinetics of test 3a-4 Q. Table 1.

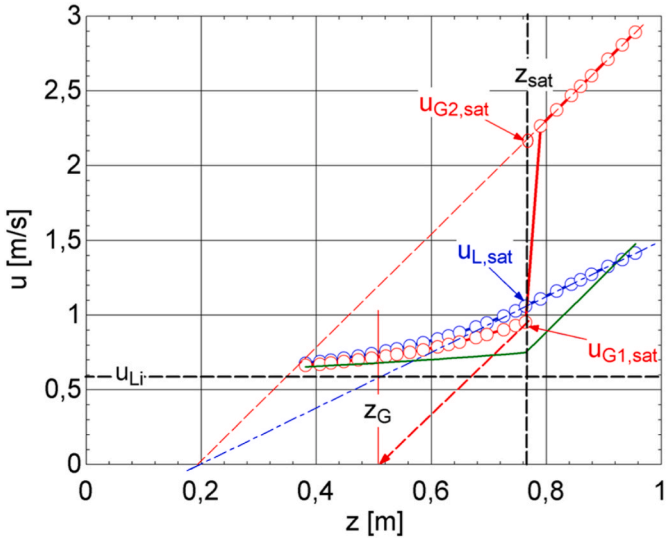

Fig. 8. Thermo-kinetics of test 3b-1 Q. Table 1.

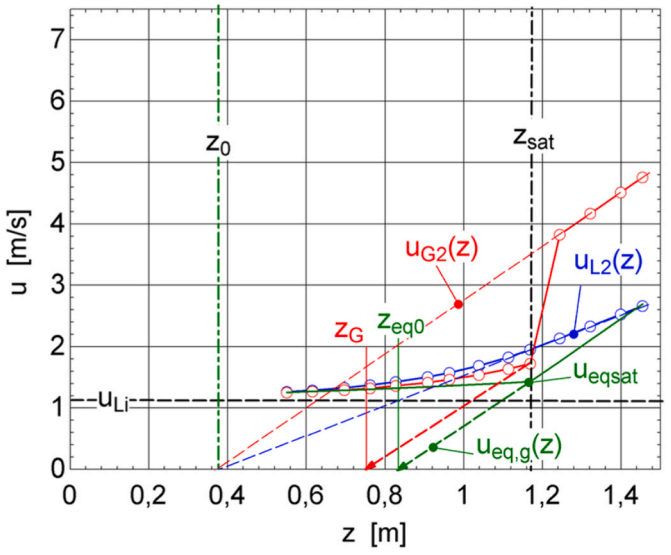

Fig. 9. Thermo-kinetics of test 3b-2 Q. Table 1.

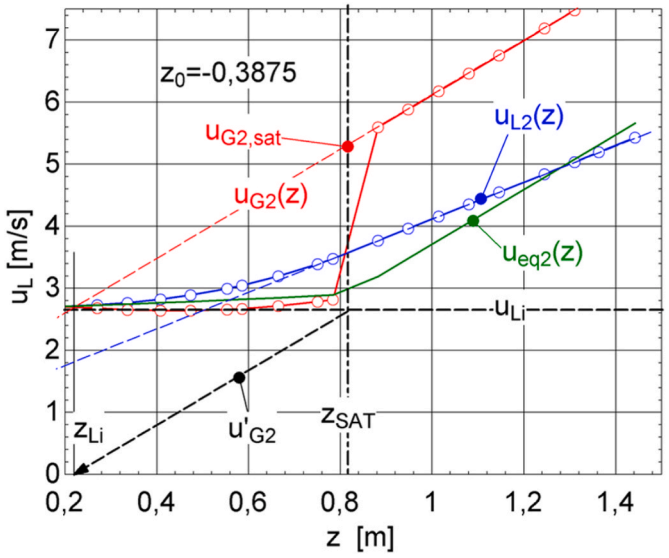

Fig. 10. Thermo-kinetics of test 3b-4 L. Table 1.

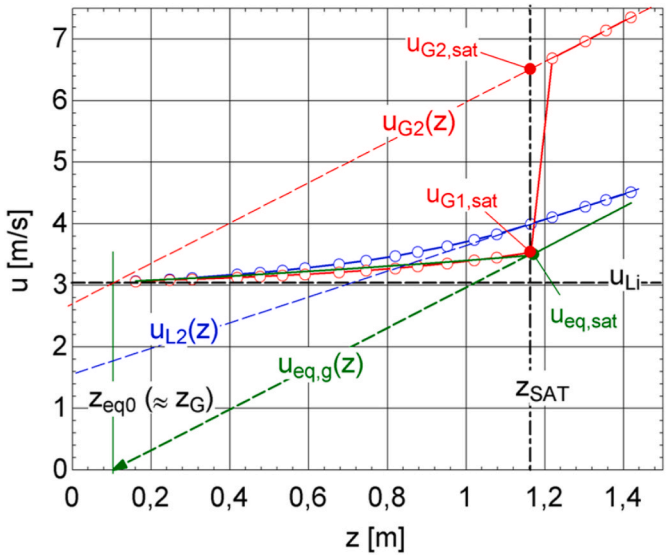

Fig. 12. Thermo-kinetics of test 2b-3 Q. Table 1.

5.5. Second equation for water at 15 MPa-Tests 2b

All the mass fluxes for tests 2b at 15 MPa are about $G \sim 2000\ kg/m^2s$, which means a u_{Li} around 3 m/s. Remark that higher the pressure, lower the saturated vapor slope u'_{G2}. Test 2b-2 Q, with a very low backward saturated vapor velocity slope $u'_{G2} = 2,27\ m^{-1}$, is analyzed in Fig. 11. Hence, backward $u_{L2}(z)$ intersects neither the subcooled equilibrium velocity $u_{eq1}(z)$ nor the inlet one u_{Li} at z_G, or much less at z_{eq0}, which now is higher than z_G. Moreover, at difference from tests set at 11 MPa, backward $u_{G2}(z)$ cannot intersect u_{Li} either at z_G or at z_{eq0}. However, from inspection of Fig. 11, a new very simple second equation is proposed for tests 2b-1 Q and 2b-2 Q

$$u_{G1,sat} = u_{Li}. \tag{39}$$

On the other hand, for test 2b-3 Q with a higher slope $u'_{G2} = 3,32\ m^{-1}$ thanks to a higher heat flux, the situation changes drastically, see Fig. 12. Now, the backward $u_{G2}(z)$ can indeed intersect u_{Li} at z_{eq0} or at z_G. The 2nd equation would be similar to that of foregoing tests with high mass flow rates i.e., 3a-3 Q, 3a-4 Q and 3b-3 L. However, for test 2b-3 Q and for test 2b-4 Q, the z-intercept z_{eq0} has supplied better results. For these two tests, we have found the same 2nd equation i.e.,

$$u_{G2}(z_{eq0}) = u_{Li} \rightarrow u_{G2,sat} = u'_{G2}(z_{sat} - z_{eq0}) + u_{Li} \rightarrow u_{G2,sat} = u_{eqsat} + u_{Li}. \tag{40}$$

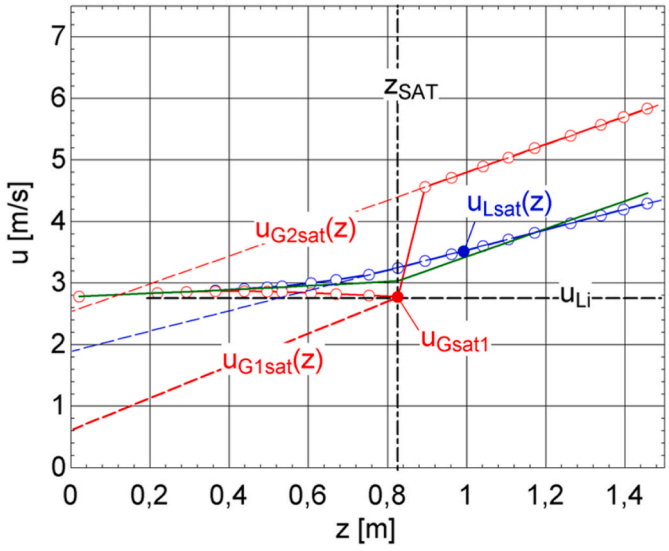

Fig. 11. Thermo-kinetics of test 2b-2 Q. Table 1.

5.6. 2nd equation for tests 4a and 4b

All tests for set 4a have similar mass flux $G \sim 1000\ kg/m^2s$ and heat flux $q'' \sim 1\ MW/m^2$ but increasing pressure equivalent to decreasing u'_{G2}, see Table 2.

Thus, test 4a-1 Q with the lower pressure (3,01 MPa) has the higher slope $u'_{G2} = 11,88\ m^{-1}$. This slope is almost the same as test 2a-5 Q, which is at 7 MPa and has $q'' = 1,98\ MW/m^2$. Besides, their mass fluxes are practically identical too ($G \sim 1000\ kg/m^2s$). Therefore, their respective 2nd equations are also equal.

Test 4a-2 Q at 4,41 MPa, has a lower slope $u'_{G2} = 7,80\ m^{-1}$ than above. After several checks, the second equation selected is based on the z-intercept z_L

$$u_{L2}(z_L) = u_{eq1}(z_L). \tag{41}$$

Test 4a-5 L, with a very high pressure (14,68 MPa), a medium inlet mass flux (1000 kg/m^{2}s) and $q'' = 1,13$ MW/m^2, has the lowest slope of the set 4a i.e., $u'_{G2} = 3,34\ m^{-1}$. On the other hand, test 4b-1 L, at 7 MPa, G = 2037 kg/m^{2}s and also $q'' = 1,13$ MW/m^2, has a slope of 6,67 m^{-1}. Finally, it has been found that both tests have the same second equation based on the z-intercept z_{eq0}

$$u_{G2}(z_{eq0}) = u_{eq,g}(z_{eq0}). \tag{42}$$

6. Searching the best ONB point with the measured void profiles and the two equations

The new simplified void profile model is function of three parameters i.e., z_{ONB}, $S_{1,sat}$, and S_2. On the other hand, we have presented two new equations, which include the above three parameters. Moreover, we have the accurate measurement of the void fraction profiles taken by MPI [20]. They could serve as 'third equation' if we looked through these data for the 'best' z_{ONB}. The best ONB point should supply the best fitting, in other words, should give the minimum absolute error between the simulation and the experimental void profile. Remark that the simplified procedure used in Ref. [27] to determine the best z_{ONB} was merely a visual inspection.

To ease the searching it would be convenient to have previously

some fair simulation of the test. An EES (Engineering Equation Solver) [30] program solves the non-linear equations system with two basic unknowns namely, $S_{1,sat}$, and S_2. Although, due to the definitions of such slip ratios, see Eqs. (18) and (19), the velocities $u_{G2,sat}$, $u_{G1,sat}$ and $u_{L,sat}$ are also solved. The inlet data to the program are the void fraction profile, the operation conditions and the selected ONB point. As we will see later, it is easy to change the second equation used in order to test the error produced and to check which slip ratio profile, the linear (L) or the quadratic (Q) one, works better.

After a second equation is selected, the program is run for several ONB points. For each z_{ONB}, the absolute error of the void simulated profile against the void data is calculated. Finally, plotting the error of the simulations against the set of z_{ONB} checked, the best ONB should give the minimum error.

6.1. Absolute error to assess the best ONB point

In principle, the mean absolute error (MAE) is used to assess the calculations, and is defined as

$$MAE = \frac{1}{n}\sum_i \left|\alpha_{i,exp} - \alpha_{i,cal}\right| \times 100\% \tag{43}$$

where $\alpha_{i,exp}$ and $\alpha_{i,cal}$ are, respectively, measured and predicted void fraction data points from some test in Table 1 with n void data. This mean absolute error shown in the last column of Table 1 has been calculated for the best ONB point found for such test (also shown in Table 1).

However, to ease the assessment of the ONB point for any test, we will use merely the sum of the absolute error SAE, defined simply as

$$SAE = \sum_i \left|\alpha_{i,exp} - \alpha_{i,cal}\right|. \tag{44}$$

The twenty-four tests measured by Bartolomei et al. [20] have been fully analyzed following this procedure and checked, at the same time, several possible options. It has been possible to find clear minima of the absolute error, which would define the best ONB point, for all the tests, see Table 1. The second equation in Table 1 is coherent with this best ONB point found. Next, some examples are shown.

6.2. Searching the best ONB point

For test 1-2 L, Fig. 13a shows the clear minima found varying z_{ONB} for the two options of the slip ratio profile i.e., linear (L) and quadratic (Q), see sub-section 3.1. Clearly, the best ONB point, which supplies the best fitting to data, is found for the linear slip ratio profile, and the parameters $S_{1,sat}$ and S_2 found for this linear option are included in Table 1.

Fig. 13b compares the void fraction profiles calculated with the best ONB found for options L and Q. It is necessary recognize that visually is difficult to distinguish both options, maybe at the extremes of the profile. Finally, to highlight that the thermal approximation $z_{1/2}$ to the ONB point, explained later, is very close to the best z_{ONB} found.

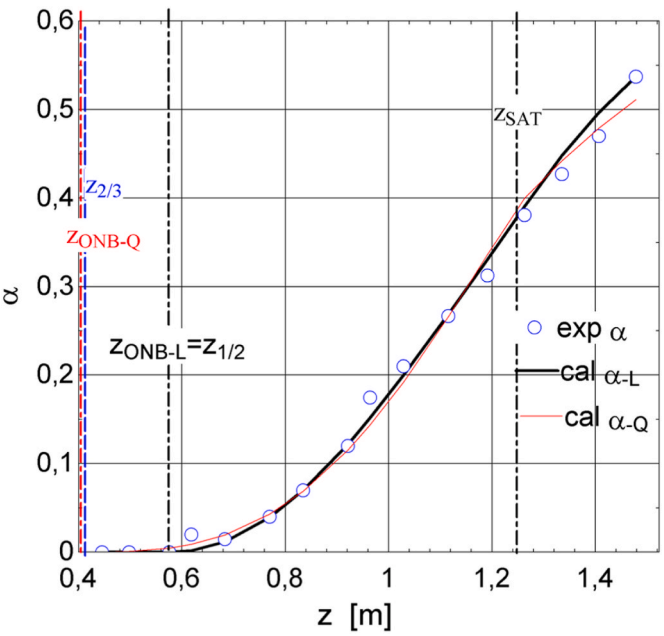

Fig. 13b. Void profiles for best z_{ONB}. Test 1-2 L. Table 1.

For test 2a-4 Q, Fig. 14a shows the clear minima found varying z_{ONB} for the L and Q options of the slip ratio profile but now also including two different second equations, see Table 1. The best ONB arises for the quadratic slip ratio with Eqs. (29) and (34). It is particularly noteworthy that every combination has its own best ONB that would seem to be more relevant than the second equation chosen. As can be seen in Fig. 14b, the void profiles with better results i.e., Q and Eqs. (29) and (34), against L and Eqs. (30) and (41) exhibit small differences. Finally, highlight that the thermal approximation $z_{1/2}$ to the ONB point is near to the best z_{ONB} found for the Q option.

For test 3a-3 Q, Fig. 15a shows the minima found varying z_{ONB} for the L and Q options also including two different second equations. The best ONB arises for the quadratic slip ratio and Eqs. (29) and (36). However, the results for Eq. (29) & Simple (36), also with the Q slip, are practically the same, see Fig. 15b. Finally, point out that the thermal approximation $z_{2/3}$ to the ONB point, explained later, is again very close to the best z_{ONB} found for the Q option. Note that in Fig. 15b has been used the same z_{ONB}

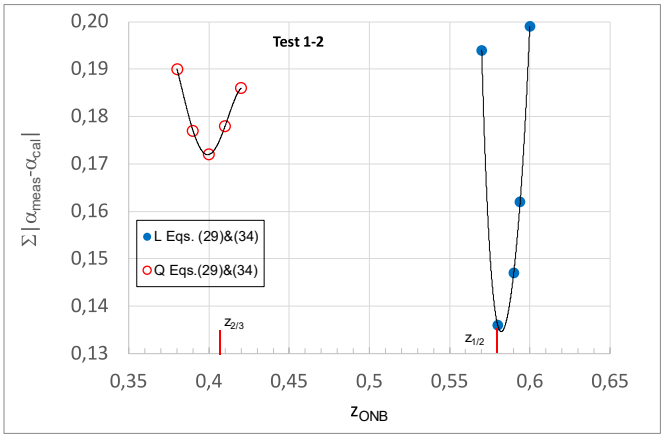

Fig. 13a. Minimum absolute error function of z_{ONB}. Test 1-2 L. Table 1.

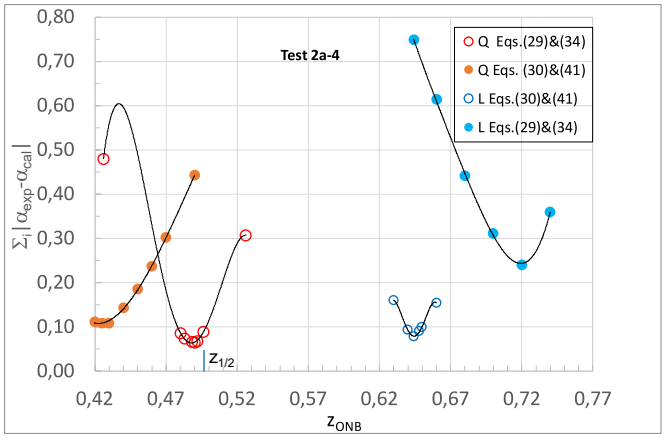

Fig. 14a. Minimum absolute error function of z_{ONB}. Test 2a-4 Q. Table 1.

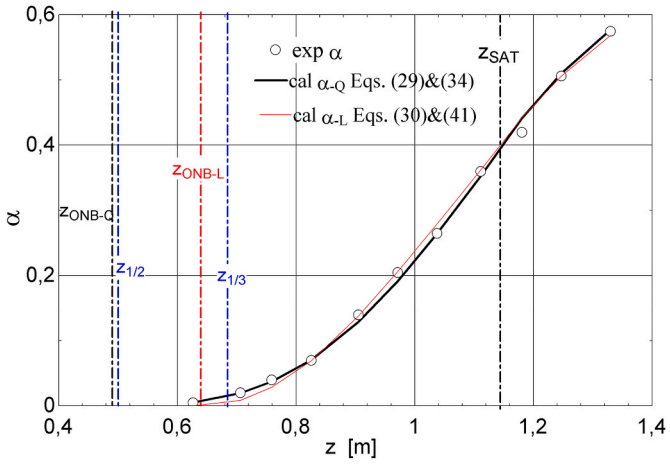

Fig. 14b. Void profiles for best z_{ONB}. Test 2a-4 Q. Table 1.

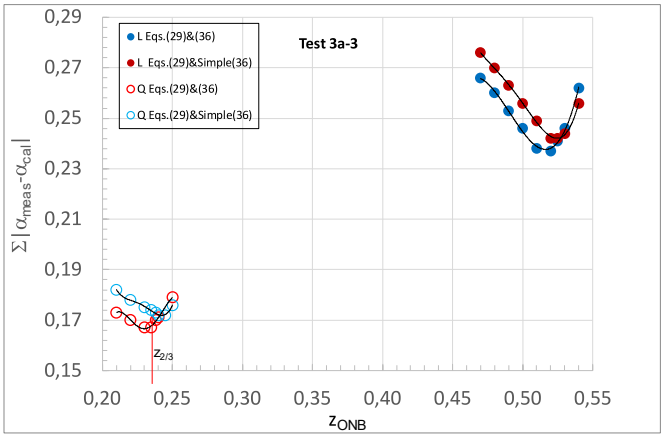

Fig. 15a. Minimum absolute error function of z_{ONB}. Test 3a-3 Q. Table 1.

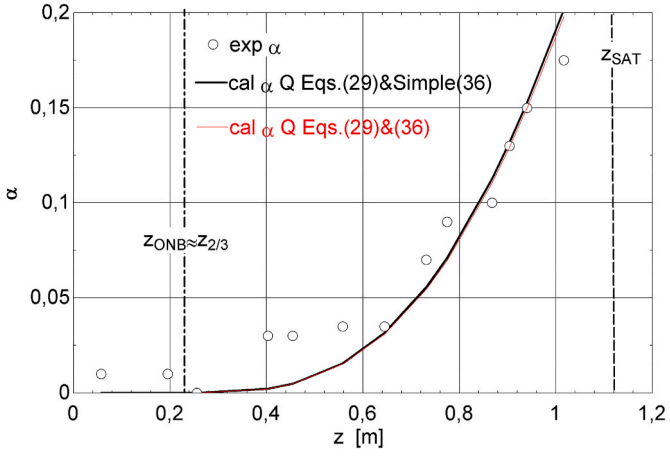

Fig. 15b. Void profiles for best z_{ONB}. Test 3a-3 Q. Table 1.

for both options.

Fig. 16a shows, for test 3b-3 Q, the minima found varying z_{ONB} for the L and Q options also including the same two different second equations as above. The best ONB arises for the Q slip but, in this case, for Eq. (29) & Simple (36). Although, the results for Eqs. (29) and (36) also with the slip option Q are very similar, see Fig. 16b. Moreover, point out that, for this test, the thermal approximation $z_{2/3}$ (−0,297 m) to the

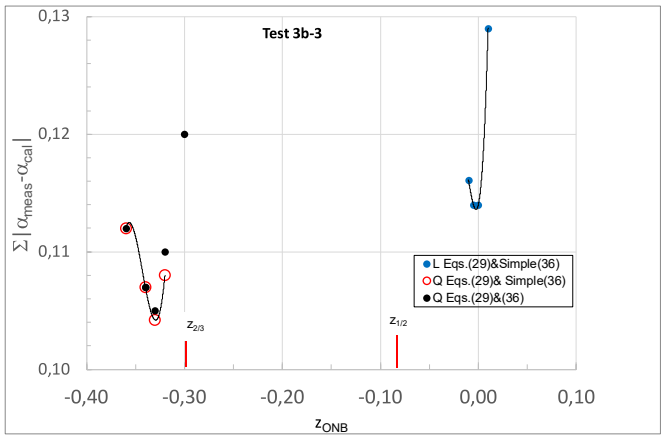

Fig. 16a. Minimum absolute error function of z_{ONB}. Test 3b-3 Q. Table 1.

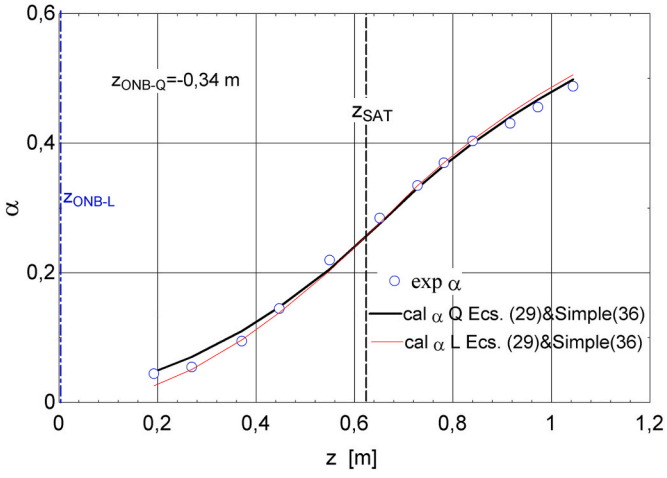

Fig. 16b. Void profiles for best z_{ONB}. Test 3b-3 Q. Table 1.

best ONB, which is explained later, is not so close to the best z_{ONB} found (−0,34 m) as the above tests. Finally, remark that the L option in Fig. 16b would also be a fair simulation option with a best ONB point equal to 0 whereas now the $z_{1/2}$ = -0,083 m is near to it.

For test 2b-4 Q, Fig. 17a presents the minima found varying z_{ONB} for the L and Q options and for two different second equations rather different between them i.e., Eqs. (33) and (40), which works with the z_{eq0}-intercept, and Eq. (29) & Simple (36) with the z_G-intercept. The

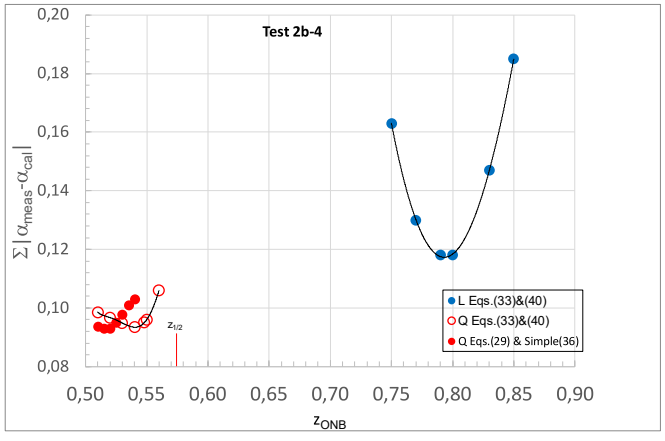

Fig. 17a. Minimum absolute error function of z_{ONB}. Test 2b-4 Q. Table 1.

errors of the best ONB found working with the Q option are almost identical although their locations are slightly different. Again, see Fig. 17b, the ONB location seems more significant than the seconds equation used. Also point out that the best ONB point (z_{eq0}) is near to $z_{1/2}$.

Fig. 18a presents, for test 4a-2 Q, the minima found varying z_{ONB} for the L and Q options and for two different second equations rather different between them i.e., Eqs. (30) and (41), which works with the z_L-intercept, and Eqs. (29) and (34) with the z_G-intercept, both with the Q option. The best ONB is clearly for the Q slip with the z_L-intercept. Fig. 18b compares the void fraction simulations for the 2nd equation options both with the Q slip profile. Here, the void prediction with the z_L-intercept is better than working with the z_G-intercept. Finally, the best ONB point (z_L) is very close to $z_{2/3}$ although the best ONB with z_G is not so close to $z_{1/2}$.

For test 4a-5 L, Fig. 19a shows the minima found varying z_{ONB} for the L and Q slip profiles also including two different second equations: one working with the z_{eq0}-intercept i.e., Eqs. (33) and (42), and the other with the z_G one i.e., Eq. (29) & Simple (36). The best ONB arises for the linear slip ratio with the z_{eq0}-intercept. Fig. 19b compares the best L option (using the second equation working with z_{eq0}) with the best Q option (z_G). Visually, they are identical, which may be related to the fact that the respective optimum ONB are very close. Furthermore, point out that $z_{1/2}$ is very close to the best z_{ONB} found for the L option.

Finally, Fig. 20a presents the analysis for test 4b-1 L, which has the same second equation as test 4a-5 L, see Figs. 19a-b. The results are very similar to this previous test, see Fig. 20b,and the thermal approximation $z_{1/3}$ results very close to the optimum ONB.

7. A new thermal approximation z_{therm} to the ONB point

As we have commented above, the onset of nucleate boiling is defined as the point where the first bubbles appear from wall nucleation sites [31]. Fig. 21 shows the axial profiles of the subcooled liquid temperature, T_L, and the wall temperature T_w for test 1-1 in Table 1. As first approximation, the wall temperature is considered constant after reaching saturation [31]. A more detailed wall temperature profile is shown in page 184 in Ref. [2].

T_L is read from tables with the liquid enthalpy, h_L, see Eq. (2) and p_i. Following [31], T_w is derived from Newton's law of cooling [32],

$$q'' = h_{conv}\Delta T_w = h_{conv}(T_w - T_L) \rightarrow T_w(z) = \frac{q''}{h_{conv}} + T_L(z), \tag{45}$$

where h_{conv} $\left[W/m^2K\right]$ is the convective heat transfer coefficient for fully developed turbulent flow in a smooth tube [32], which here is calculated

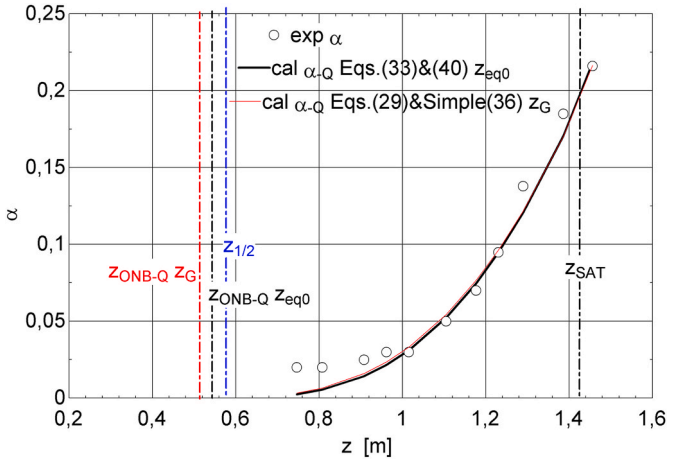

Fig. 17b. Void profiles for best z_{ONB}. Test 2b-4 Q. Table 1.

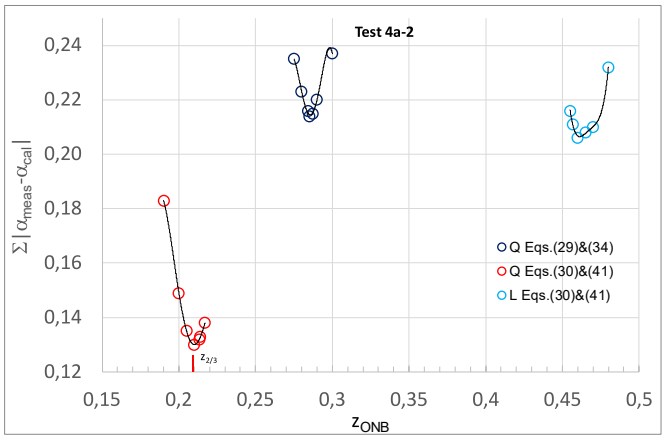

Fig. 18a. Minimum absolute error function of z_{ONB}. Test 2a-4 Q. Table 1.

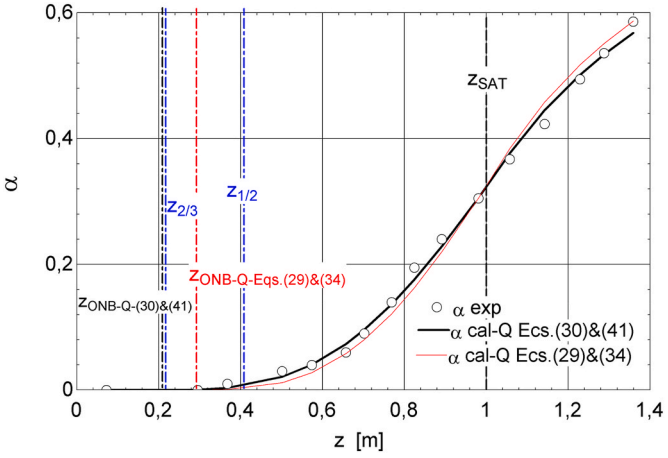

Fig. 18b. Void profiles for best z_{ONB}. Test 4a-2 Q. Table 1.

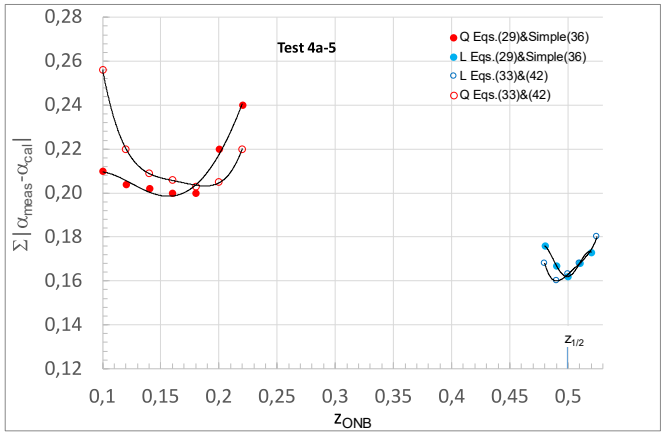

Fig. 19a. Minimum absolute error function of z_{ONB}. Test 4a-5 L. Table 1.

by the Dittus-Boelter correlation [31,32],

$$\frac{h_{conv}D}{k_L} = 0.023 Re_L^{0.8} Pr_L^{0.4}, \tag{46}$$

where k_L is the conductivity, Re_L the Reynolds number and Pr_L the Prandtl number, all calculated for subcooled liquid. In Eq. (46) the liquid properties are evaluated at the average liquid temperature between the inlet and saturation.

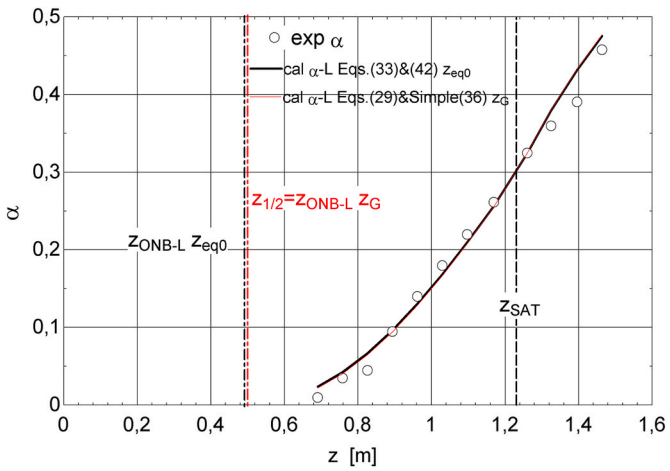

Fig. 19b. Void profiles for best z_{ONB}. Test 4a-5 L. Table 1.

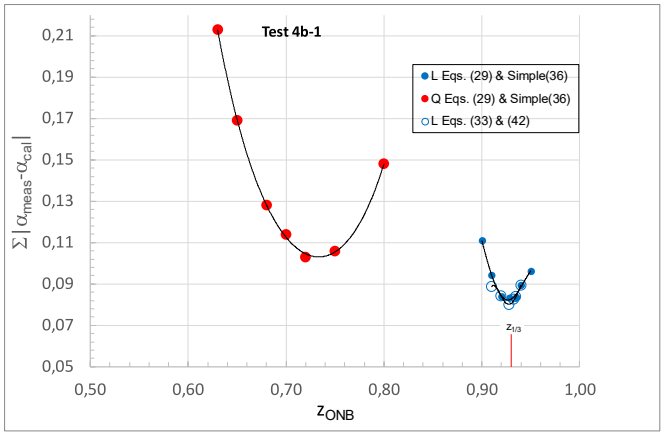

Fig. 20a. Minimum absolute error function of z_{ONB}. Test 4b-1 L. Table 1.

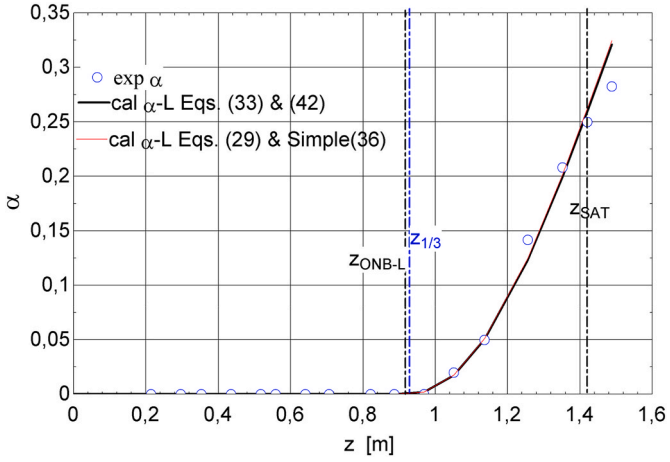

Fig. 20b. Void profiles for best z_{ONB}. Test 4b-1 L. Table 1.

The suggested thermal approximation to ONB is the point $z_{1/2}$, defined in Fig. 21, as the location that verifies the following equation

$$\Delta T_{sat} = (T_w - T_{sat}) = \Delta T_{sub} = \left(T_{sat} - T_{L,ONB}\right) \rightarrow T_{L,ONB}\left(z_{1/2}\right) = T_{sat} - \frac{1}{2}\Delta T_w. \quad (47)$$

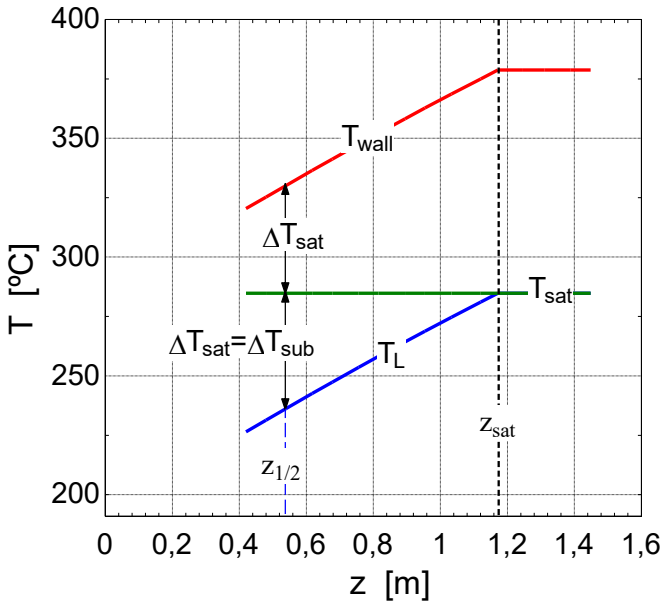

Fig. 21. Definition of $z_{1/2}$ point as a thermal approximation to ONB location. Test 1-1 L. Table 1.

Eq. (47) allows to calculate the liquid temperature that verifies the above equality. Then, the corresponding location $z_{1/2}$ can be worked out from the single flow heat balance, Eq. (2). Other possible thermal approximations to ONB, all of them called z_{therm}, would be $z_{2/3}$ and $z_{1/3}$, see Table 1, defined as

$$T_L\left(z_{2/3}\right) = T_{sat} - \frac{2}{3}\Delta T_w; \quad T_L\left(z_{1/3}\right) = T_{sat} - \frac{1}{3}\Delta T_w. \quad (48)$$

Clearly, $z_{2/3}$ would be before $z_{1/2}$, and $z_{1/3}$ after $z_{1/2}$.

A possible justification for the foregoing thermal approximation $z_{1/2}$ could be the following. To reach saturated vapor (bubbles), bulk liquid at temperature T_L has to be first heated until saturated liquid to overcome the subcooling, ΔT_{sub}. Then, it changes of phase from saturated liquid to saturated vapor thanks to the wall superheat ΔT_{sat}. Just before the first stable bubble arise after the ONB point, the bubbles would condense to saturated liquid releasing the heat to the surrounding cooler bulk liquid. If this condensing heat was equivalent to the previous boiling heat, as suggested by Griffith, Clark and Rohsenow [29], the water would come back to saturated liquid if $\Delta T_{sub} = \Delta T_{sat}$. In other words, there would be the exact wall superheating to maintain the saturated liquid phase.

The 'best' ONB locations, which are shown in Table 1 and have been explained in the previous section 6, should be compared with the column $z_{ONB} = f \cdot z_{therm}$, which is to the left of best z_{ONB} (m) in Table 1. The column $f \cdot z_{therm}$ shows the relation between the above suggested thermal approximation and the 'best' z_{ONB} thus allowing to assess the actual accuracy of the thermal approximation.

8. Results and discussion

The solution of the non-linear two equation system, including the searching of the best ONB point, has supplied the three main parameters (z_{ONB}, $S_{1,sat}$, S_2) that allow to plot the void fraction profile as commented in sections 2 and 3. As main result of this work, Figs. 22–28 show an acceptable modeling of the twenty-four void fraction experimental profiles reported by Bartolomei et al. [20] for water flowing upwards through a vertical uniformly heated tube. The tests gathered for each figure have similar operating conditions (see Table 1).

As we have already remarked above, for the true volumetric steam content α, determined by γ-radiation, the maximum absolute experi-

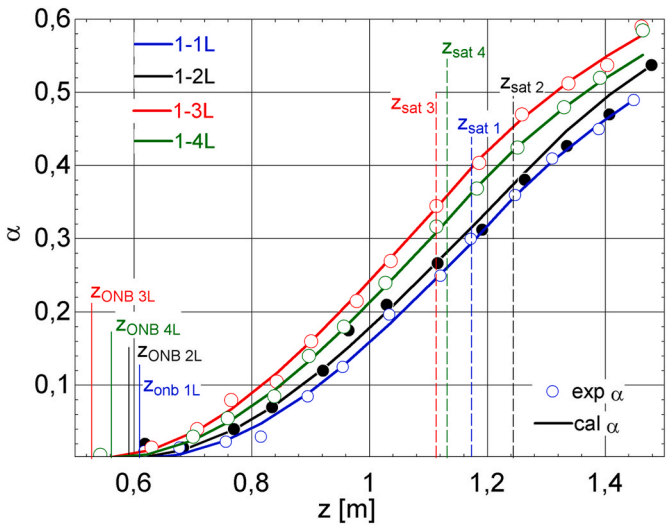

Fig. 22. Void fraction profiles for tests 1 & 7 MPa. Table 1.

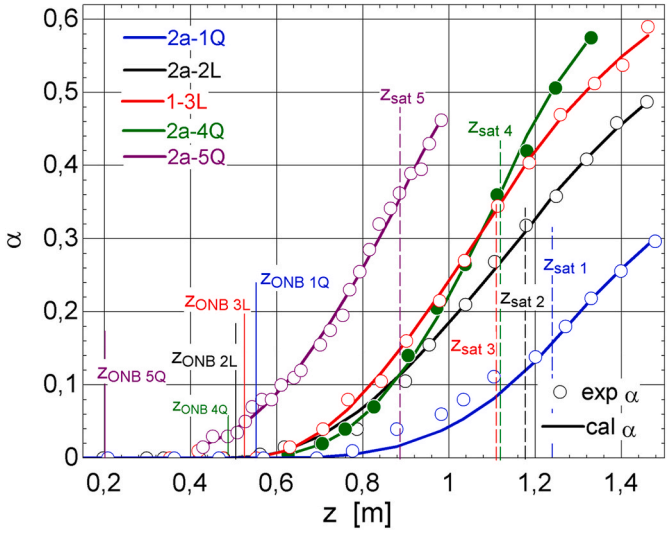

Fig. 23. Void fraction profiles for tests 2a & 7 MPa. Table 1.

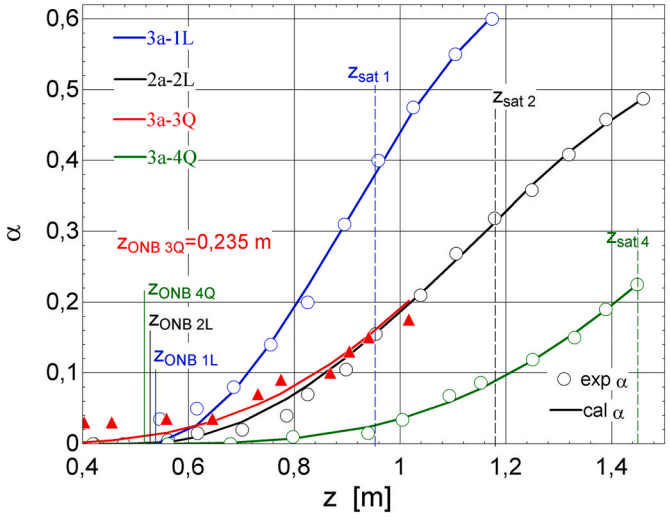

Fig. 24. Void fraction profiles for tests 3a & 7 MPa. Table 1.

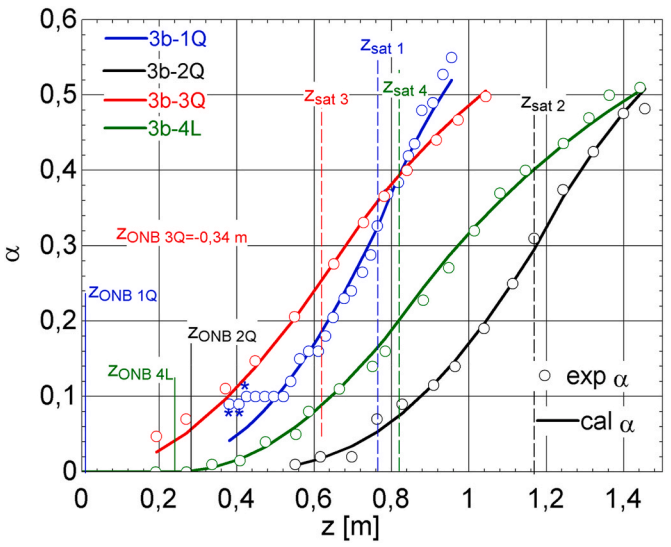

Fig. 25. Void fraction profiles for tests 3b & 11 MPa. Table 1.

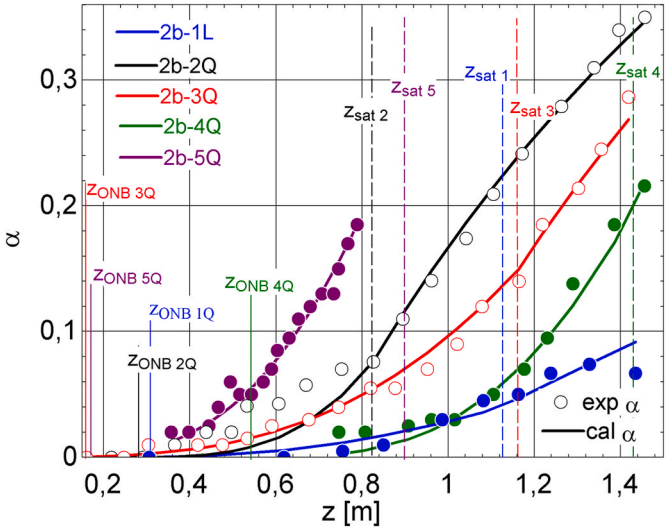

Fig. 26. Void fraction profiles for tests 2b & 15 MPa. Table 1.

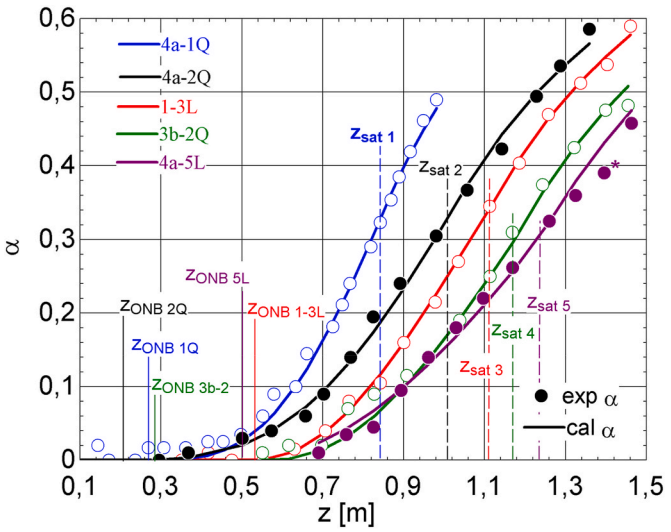

Fig. 27. Void fraction profiles for tests 4a & 1000 kg/m^{2}s Table 1.

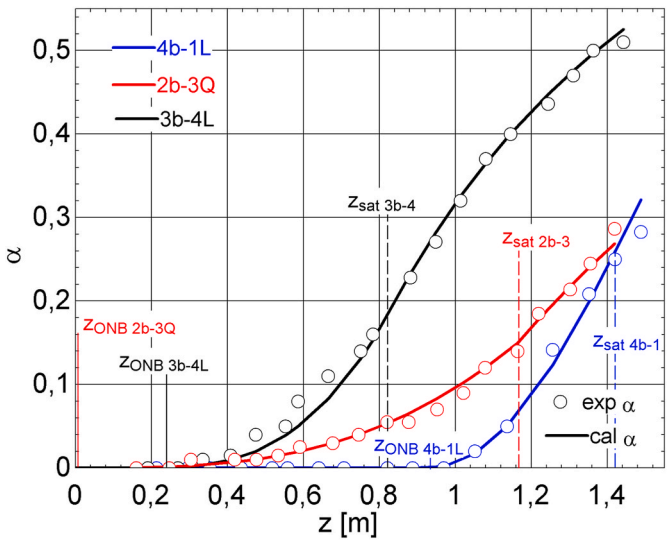

Fig. 28. Void fraction profiles for tests 4b & 2000 kg/m^{2}s Table 1.

mental error did not exceed ± 0.04 [20]. For the large majority of data, the maximum absolute difference ($\Delta\alpha = |\alpha_{meas.} - \alpha_{cal.}|$) between the measured void value and the simulated one is lower than 0.04 (4%). There are only two tests that have some simulated void point with Δα greater or equal to 4 % namely, tests 3b-1 Q (4,9%) in Figs. 25 and 4a-5 L (4,1%) Fig. 27 where the respective points are marked with an asterisk. Moreover, as we have already commented above, the last column of Table 1 shows the mean absolute error, see Eq. (43), for each test.

Therefore, this simplified 3-parameter model exhibits clear advantages over the previous 5-parameter model presented elsewhere [27]. First, this 3-parameter model only needs the ONB location, which has been found minimizing the absolute error. Notice that the five-parameter model needed not only the ONB but also the onset of significant void (OSV) and its vapor content, which would mean a large amount of work and uncertainty. Moreover, besides the ONB, the OSV and the α_{OSV} were also varied finding the better fitting of data merely by visual inspection. Finally, at difference of the two thermo-kinetic equations presented here, which have been compared with the 24 MPI tests, the two thermo-kinetic equations suggested in Ref. [27] were not fully verified because only eight out of the 24 were checked.

8.1. Importance of accurate ONB. Thermal approximation

The best locations of the onset of nuclear boiling (z_{ONB}) used for void profile simulations, see Table 1, have been also highlighted in Figs. 22–28. Remember that these locations have been found minimizing the absolute error also trying different options of the slip ratio profile and the second equation used.

From the foregoing analysis in section 6, it would seem clear that the precise location of this ONB is quite important for the accuracy of the simulation. Indeed, the best ONB location is much more significant than the slip ratio option, see for example Figs. 13b, 14b, and 16bb, etc., or that the second equation chosen, see Figs. 14b, 15b, and 17bb, etc. Moreover, it has been several times verified, see section 6, that there are many tests in which thermal approximations are quite near to the best ONB.

Unfortunately, the thermal approximations suggested in section 7 i. e., $z_{2/3}$, $z_{1/2}$ and $z_{1/3}$, only reach the needed accuracy to reproduce correctly the void fraction profile in some few tests. For test 1-1 L, Fig. 29 compares the void fraction profile (red line) calculated with origin in the thermal approximation to ONB i.e., $z_{1/2}$ (=0,544 m), with the void fraction data (circles) and the simulation (bold black line) using the best z_{ONB} (0,608 m). The absolute error, denoted by Δ, is the absolute difference, as a percentage, between data and the calculation with $z_{1/2}$. Remark that he maximum Δ for test 1-1 L simulated with the 'best' z_{ONB} (m) was 1,7%. Now, not only the maximum is 9,2%, more than five times the previous error, but also almost upper half of the $z_{1/2}$ void profile has an error around 8%.

As we have already commented in the introduction, standard models neglect the first zone of flow boiling, with $\alpha \leq 2-4\%$ [15], and practically commences later, at the onset of significant void (OSV) [8]. Also remark the current importance given to calculate the OSV accurately for predicting the axial void fraction profile [5–7,12–14].

In view of the analysis of section 6, and the comparison shown in Fig. 29, little shifts from the best ONB could mean significant deviations from data. Thus, it is clear, as it happens with the OSV in standard models, that the accurate calculation of the ONB would also be of the outmost importance for a good prediction of the void profile.

However, as can be seen in Table 1, in the column of the best z_{ONB} in function of $z_{2/3}$, $z_{1/2}$, $z_{1/3}$, etc., some of these thermal approximations are not far from the 'best' fitting locations. Therefore, a reasonable starting point for searching the 'best' ONB could be some thermal approximation.

8.2. Two options to calculate the slip ratio profile along subcooled flow boiling

With the simplified model presented here, the full subcooling flow has been simulated with only one zone, provided we have a good estimation of the ONB. This has been possible due to the selection of one of the two new slip ratio functions suggested for subcooled boiling i.e., a linear function (L) and a quadratic one (Q), see Eqs. (16) and (17), respectively.

For test 2a-5 Q, see Table 1, Fig. 30 shows the void fraction profiles calculated with the linear slip (fine red line) and the quadratic one (bold black line). The profiles logically differ at the beginning but they converge approximately towards the middle of the subcooled region. Here the selection has been the quadratic slip, with the lower best ONB location, that supplies the best simulation of the subcooling flow beginning. The thermal approximation suggested in this work ($z_{1/2}$) has resulted relatively close to the best z_{ONB} of the quadratic slip function.

Apparently, in Fig. 30, it could be thought that the option Q and the option L would give similar results. However, again, the appropriate location of the best ONB for each slip profile option is crucial. Indeed, the best z_{ONB} found for the two options are rather different each other. Therefore, the selection of a linear or a quadratic slip profile would be as

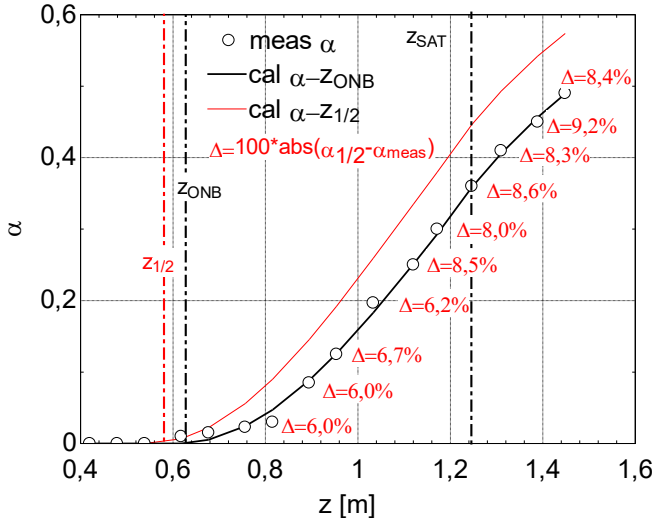

Fig. 29. Void fraction profiles with origin the best-z_{ONB} and the thermal approximation $z_{1/2}$. Test 1-1 L. Table 1.

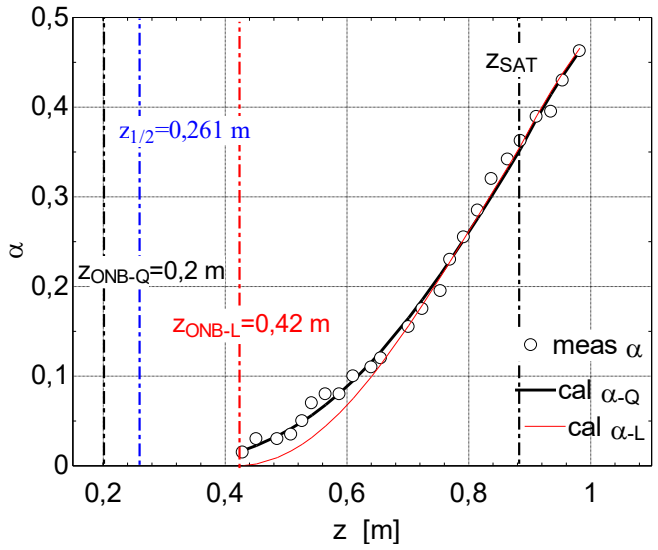

Fig. 30. Void fraction profiles from linear and quadratic slip ratios. Test 2a-5 Q. Table 1.

correct as its associated best z_{ONB} be.

Unfortunately, it is not yet clear how to choose the correct slip ratio function. From the results, see Figs. 22–28, it would seem that linear slip profiles would imply that void fraction appears not close to the inlet, more or less suddenly, then its growing is fast and the full subcooling profile is almost linear. On the other hand, for quadratic profiles, low (although significant) void fraction arises close to the beginning, its growing is slow and the subcooling profile resembles a quadratic curve, see, for example, tests 2a-1 Q and 2a-5 Q in Fig. 23.

For all the tests in set 1 (7 MPa), their slip profiles are linear, see Table 1. They have medium mass flux, high heat flux and high subcooling. Test 4b-1, with the same pressure and heat flux, has half the subcooling of tests in set 1, which could favor the early arising of bubbles, but twice the mass flux, which could delay the first bubbles onset. Finally, the linear slip has given the best results for test 4b-1, which could indicate that the two opposing trends would have been balanced. On the other hand, a high heat flux would promote a fast onset and vice-versa. It would be the combination of these three factors, and probably with the pressure too, that would define the selection of the slip ratio profile.

8.3. Some possible justification of the second equation. Selection of the correct equation

One of the most significant findings of this work is the new relations found between the saturated vapor and liquid velocities with the 'equilibrium' and the inlet velocities, when such saturated velocities are reversed to subcooled flow zone. Due to the liquid continuity and uniform heat flux, it is assumed that the reversing saturated liquid is the backward linear extension, see Fig. 4 dashed blue line, of the saturated liquid velocity $u_{L2}(z)$ (blue line) with slope u'_{G2}/S_2. Indeed, this backward liquid velocity crosses saturation at $u_{L,sat}$ too.

On the other hand, in the original process, the vapor velocity jumps from $u_{G1,sat}$ to $u_{G,sat}$ when passing through saturation. This could justify that, in reversing the vapor process, the saturated vapor velocity can arise at saturation taking at least three different velocities. Namely, from the highest to the lowest one, $u_{L,sat}$, $u_{G1,sat}$ and u_{eqsat}. So, three possible linear trajectories, with the same slope u'_{G2}, of the reverse saturated vapor from saturation towards subcooled boiling would be: the dashed blue arrow line denoted $u_{L,g}(z)$ with origin $u_{L,sat}$, the dashed red arrow line $u_{G1}(z)$ beginning at $u_{G1,sat}$, and the dashed green arrow line called $u_{eq,g}(z)$ and crossing saturation by u_{eqsat}.

The second equation suggested here arises from assuming that the z-intercept of these possible three trajectories of the reverse saturated vapor i.e., z_L, z_G and z_{eq0}, may be also the abscissa of some relevant intersection. A possible logic behind the second equation is commented in the following.

For several tests, it has been certainly checked that z_G, Eq. (29), is also the abscissa of a useful intersection. Remark that the z_G intercept is the duct axis location where vapor reversing velocity becomes zero. For the four tests of the first set in Table 1 i.e., 1-1 L, 1-2 L, etc., in addition of tests 2a-4 Q and 3a-1 L, the second equation would suggest that this z_G is also the point where the backward extension of $u_{L2}(z)$ (dashed blue line) would intersect the subcooled equilibrium velocity profile $u_{eq1}(z)$, Eq. (34). This would make a certain amount of sense because when the reverse liquid velocity reached the subcooled liquid thermodynamic equilibrium velocity, following the definition of 'equilibrium' velocity in subsection 5.2, the reverse vapor velocity should become zero. Additionally, a similar logic could be applied to other tests.

In spite of the variety of options found for the second equation, the selection of the specific second equation would not seem arbitrary.

First, for some extreme tests with very low heat flux, the second equation would be quite simple. At 7 MPa and $G \sim 1000\ kg/m^2s$, the lowest heat flux is $q'' = 0{,}44\ MW/m^2$ for test 2a-1 Q, with 2nd equation being merely $z_0 = 0,0\ m$. At 15 MPa and $G \sim 2000\ kg/m^2s$, the lowest heat flux is now $q'' = 0{,}42\ MW/m^2$ for test 2b-1 L, and the second equation, Eq. (39), is also very simple: $u_{G1,sat} = u_{Li}$. Test 2b-2 Q, with the same pressure and mass flux but $q'' = 0{,}77\ MW/m^2$, has the same 2nd equation.

On the other hand, for the test 2b-5 Q, with the highest heat flux $q'' = 2{,}21\ MW/m^2$, at 15 MPa and $G \sim 2000\ kg/m^2s$, the second equation would be also quite simple: $u_{G2}(z_{1/2}) = 0$.

Second, for 7 MPa, mass flux of about 1000 kg/m^{2}s, and the slope u'_{G2} in the range 6,61 to $10,13\ m^{-1}$ the second equation could be Eqs. (29) and (34). Test 3a-1 L also verifies the same second equation although with a lower slope ($4{,}62\ m^{-1}$) but half the above mass flux, see Fig. 6.

Third, for mass flux of around 1500-2000 kg/m^{2}s, Eqs. (29) and (36) or its equivalent i.e., Eq. (29) & Simple (36), with z-intercept z_G, would verify the tests 3a-3 Q and 3a-4 Q, at 7 MPa and with slopes 4,50 and 4,62 m^{-1}, respectively; also test 3b-3 Q at 10,81 MPa and $u'_{G2} = 4{,}54\ m^{-1}$. Besides, some tests at high pressures and mass fluxes, with z-intercept z_{eq0}, could be alternatively simulated with the same equations Eq. (29) & Simple (36) following the analysis of section 6. For example, test 2b-4 Q at 14,7 MPa and slope $5{,}07\ m^{-1}$; test 4a-5 L at 14,68 MPa, G = 1000 kg/m^{2}s, and $u'_{G2} = 3{,}34\ m^{-1}$; and test 4b-1 L at 7 MPa, about 2000 kg/m^{2}s and slope $6{,}67\ m^{-1}$. Also remark that for these tests with z_{eq0}-intercept, the best ONB corresponding to the z_G-intercept alternative is very near to the original second equation in Table 1, see section 6.

Finally, for the two tests with the highest slopes namely, test 2a-5 Q with $u'_{G2} = 11{,}40\ m^{-1}$ (7 MPa, $G \sim 1000\ kg/m^2s$, $q'' = 1{,}98\ MW/m^2$), and test 4a-1 Q with $u'_{G2} = 11{,}88\ m^{-1}$ (3 MPa, $G \sim 1000\ kg/m^2s$, $q'' = 0{,}98\ MW/m^2$) the second equation is the same: $z_0 = z_{1/3} - (u_{Li}/u'_{G2})$.

Clearly, it would be necessary to analyze much more cases and checking the possible equivalences to complete the options and confirm this very preliminary selection of the 2nd equation.

8.4. Limitations of the model proposed

As pointed out above, although the void fraction profiles simulations have been acceptable, these results should be taken with extreme care since much more tests have to be analyzed to confirm the second equation found and its selection.

On the other hand, it is necessary to notice about the rather strong influence of small shifts of the ONB location on the accuracy of the simulated void fraction profile, see subsection 8.1. Therefore, a clear and accurate procedure to find the best ONB location remains. For example,

the influence of the inlet subcooling on the ONB, which is not addressed in this work, should be taken into account.

Also, the criteria for selecting of the slip ratio profile along subcooling i.e., a linear or a quadratic function, lack. As we have advanced above, the combinations of subcooling, mass flux and heat flux could be the key.

Moreover, remark that the second equation proposed is based on assuming linear reversing of the saturated liquid and vapor velocities. This could be more or less acceptable for a uniformly heated pipe. Under non-uniform heating e.g., sinusoidal one, the second equation, if it existed, could be completely different and much more complicated.

Finally, it is necessary to notice about the limitations of the present model with regards to geometry since the model has been only checked against tests with one geometry i.e., vertical upwards flow boiling of water through a circular tube. As we have already commented in the introduction, in Ref. [4], they have been provided recent developments of the drift-flux type correlations in large-size channels, checked against data, where the flow channel geometries analyzed were very varied: circular, annulus, rectangular, square, vertical rod bundle, and horizontal rod bundle.

9. Conclusions

A new steady one-dimensional void fraction profile model for subcooled-bulk flow boiling is presented in this work. The new model is based on new mass and energy balances for steady 1d non-equilibrium flow boiling developed by the author elsewhere [22,23,26,27]. The new balances are the base for a new procedure to predict the void fraction profile along subcooled and bulk flow boiling.

The prediction of the void profile is equivalent to calculate the mixture enthalpy profile that is defined through the classic thermodynamic quality, which explicitly includes the void fraction. A new energy balance, made up of such mixture enthalpy, is proposed, see Eqs. (13)–(15). Based on previous works, the main novelty of the heat balance is the explicit inclusion of the slip ratio dividing the heat applied [22,23,26,27].

For the twenty-four tests presented by Bartolomei et al. [20], it has been verified that the slip ratio profile from the beginning (the ONB) until bulk flow can be simulated with only three parameters. Namely, the onset of nucleate boiling (ONB), the slip ratio just at saturation coming from subcooling flow, $S_{1,sat}$, and the assumed constant slip ratio along bulk flow, S_2.

Therefore, a new three thermo-kinetic equations non-linear system, which include these three parameters, have been suggested. The non-linear equation system has been solved with the EES (Engineering Equation Solver) [30], which is a standard for thermo-fluid engineering. The three equations are the following:

- The continuity of the first derivative of the liquid velocity just at saturation. Following the new mass balance, the liquid velocity is considered the representative two-phase flow velocity. In this work, this equation, first presented elsewhere [27] for a five parameters model, is adapted to the new simplified model with only three parameters.
- The assumption of a theoretical linear reversion of the liquid and vapor velocities profiles from bulk flow boiling towards subcooled boiling, and their intersections with a theoretical 'equilibrium' liquid velocity along subcooling, or with the inlet velocity. This has provided new equations for the key saturated velocities that make up $S_{1,sat}$ and S_2, see Eqs. (18) and (19). The new equations found are shown in Table 1.
- The accurate measurement of the void fraction profiles taken by MPI [20] has served as a 'third equation' looking, for each simulated test, the best z_{ONB} i.e., that minimized the absolute void fraction profile simulation error.

The model has given acceptable void fraction profile simulations, see Figs. 22–28, for the twenty-four tests from MPI [20] provided a good ONB location is available. However, the model should be used with care due its current limitations:

- There is not an accurate procedure to predict yet the best location of the boiling onset exclusively based on operating conditions. Indeed, it has been verified that small changes in the location of the ONB trigger the absolute error in the void profile predictions. The prediction of ONB should be refined including the influence of subcooling not addressed in this work. However, some thermal approximations to the ONB, for example $z_{1/2}$, based on MIT classic works [29], have been also explored. They would be good starting point of the best ONB searching.
- Criteria for selecting the slip ratio function (linear or quadratic one) along subcooling flow are lacking. It is thought that subcooling levels combined with mass and heat fluxes could help in the correct selection.
- The selection of the second equation should be refined analyzing much more tests and searching for equivalences between different options. However, in spite of the quite different second equations found, see Table 1, the selection of the specific second equation for a particular test would not seem arbitrary. It could be governed by the combination of the inlet velocity and the slope u'_{G2}, last one depending on pressure, heat flux and diameter of the duct.
- The model has been only checked for only one geometry i.e., vertical upwards water flow boiling through a circular tube. Point out that there are recent drift-flux advances [4,5,16–18] for a large variety of sizes and geometries channels including circular, annulus, rectangular, square, vertical rod bundle, and horizontal rod bundle.

Finally, comment that the full **Simulation for test 1-1 L** with EES [30] can be found in the supplementary material of this work. **Simulation for test 1-1L** shows all the thermodynamic properties and the necessary equations to pose and solve the non-linear system equation suggested in this work.

Data availability statement

The data that supports the finding of this study are openly available at https://www.webofscience.com/wos/woscc/full-record/WOS:A1982PP23000005, Ref. [20].

Funding

This research did not receive any specific grant from funding agencies in the public, commercial, or not-for-profit sectors.

Declaration of competing interest

The authors declare that they have no known competing financial interests or personal relationships that could have appeared to influence the work reported in this paper.

Appendix A. Calculation of $x_1'(z_{sat})$ (along subcooling)

Appendix A1. Calculation of $x_1'(z_{sat})$ along subcooling for $S_1(z)$ a linear function

First, the thermodynamic quality along the subcooling zone (1) is derived from the mixture enthalpy definition, Eq. (10), then the first derivative can be calculated,

$$x_1(z)=\frac{h_{m1}(z)-h_L(z)}{h_G-h_L(z)}\rightarrow\ x_1'(z)=\frac{\left[h_{m1}'(z)-h_L'(z)\right](h_G-h_L(z))+h_L'(z)[h_{m1}(z)-h_L(z)]}{[h_G-h_L(z)]^2}. \tag{A1.1}$$

As we have advanced in subsubsection 1.1.1, the subcooled liquid enthalpy is calculated from the single flow heat balance, Eqs. (2) and (3), thus its derivative is equal to $q(kJ/kgm)$,

$$h_L(z)=qz+h_{Li}\rightarrow\ h_L'=q. \tag{A1.2}$$

Now, the first derivative of the mixture enthalpy along subcooling is obtained from the new simplified mixture heat balance along subcooling, see Eq. (15),

$$h_{m1}'(z)=\frac{q\left[S_1(z)-S_1'(z)(z-z_{ONB})\right]}{S_1^2(z)}=\frac{q}{S_1^2(z)}, \tag{A1.3}$$

where the definition of the new linear subcooling slip function, Eq. (18) has been used.

Finally, Eqs. (A1.2) and (A1.3) have been substituted into Eq. (A1.1), which is evaluated at saturation

$$x_1'(z)=\frac{q}{[h_G-h_L(z)]}\left[\frac{1}{S_1^2(z)}-1+x_1(z)\right]\rightarrow x_1'(z_{sat})=\frac{q}{(h_G-h_F)}\left[\frac{1}{S_{1,sat}^2}-1+x_{sat}\right] \tag{A1.4}$$

where $x_{sat}=x_1(z_{sat})$, and, previously in Eq. (A1.1), $[h_{m1}(z)-h_L(z)]$ has been substituted by $x_1(z)[h_G-h_L(z)]$ from the mixture enthalpy definition.

Appendix A2. Calculation of $x_1'(z_{sat})$ along subcooling for $S_1(z)$ a quadratic function

Although the slip ratio is now a quadratic function, the first two equations of the above Appendix A1, which do not include the slip ratio, are identical.

However, the derivation of the mixture enthalpy, which is an explicit function of the slip function, logically changes and this derivation is now evaluated at saturation taking into account Eq. (19),

$$h_{m1}'(z_{sat})=\frac{q\left[S_{1,sat}-S_1'(z_{sat})(z_{sat}-z_{ONB})\right]}{S_{1,sat}^2}=\frac{q\left[2-S_{1,sat}\right]}{S_{1,sat}^2}. \tag{A2.1}$$

Finally, Eqs. (A2.1) and (A1.2) are substituted into Eq. (A1.1), which is evaluated at saturation,

$$x_1'(z_{sat})=\frac{q}{(h_G-h_F)}\left[\frac{(2-S_{1,sat})}{S_{1,sat}^2}-1+x_{sat}\right]. \tag{A2.2}$$

Appendix A. Supplementary data

Supplementary data to this article can be found online at https://doi.org/10.1016/j.ijthermalsci.2026.110845.

Data availability

The authors do not have permission to share data.

References

[1] A.E. Bergles, J.G. Collier, J.M. Delhaye, G.F. Hewitt, F. Mayinger, Two-Phase Flow and Heat Transfer in the Power and Process Industries, Hemisphere, Washington, USA, 1981.

[2] J.G. Collier, J.R. Thome, Convective Boiling and Condensation, third ed., Oxford University Press, Oxford, UK, 1994.

[3] R.T. Jr. Lahey, F.J. Moody, The Thermal Hydraulics of a Boiling Water Nuclear Reactor, second ed., American Nuclear Society, La Grange Park, USA, 1993. Chapter 5.

[4] T. Hibiki, P. Ju, S. Rassame, S. Miwa, X. Shen, T. Ozaki, Channel size effects on drift-flux parameters for adiabatic and boiling two-phase flows, Int. J. Heat Mass Tran. 185 (2022) 122410.

[5] X. Shen, T. Yamamoto, K. Nakajima, T. Hibiki, A full-flow-range drift-flux model for adiabatic and boiling two-phase flows in vertical narrow rectangular flow channels, Int. J. Therm. Sci. 202 (2024) 109086.

[6] N. Zuber, J.A. Findlay, Average volumetric concentration in two-phase flow systems, J. Heat Tran. 87 (1965) 453–468.

[7] P. Saha, N. Zuber, Point of net vapor generation and vapor void fraction in subcooled boiling, Int. Heat Transfer Conf. Digital Library 4 (1974) 175–179.

[8] C. Cai, I. Mudawar, H. Liu, X. Xi, Assessment of void fraction models and correlations for subcooled boiling in vertical upflow in a circular tube, Int. J. Heat Mass Tran. 171 (2021) 121060.

[9] S.L. Sharma, M. Ishii, T. Hibiki, J.P. Schlegel, Y. Liu, J.R. Buchanan Jr., Beyond bubbly two-phase flow investigation using a CFD three-field two-fluid model, Int. J. Multiphas. Flow 113 (2019) 1–15.

[10] Y. Liao, E. Krepper, D. Lucas, A baseline closure concept for simulating bubbly flow with phase change: a mechanistic model for interphase heat transfer coefficient, Nucl. Eng. Des. 348 (2019) 1–13.

[11] D. Mitrakos, A. Vouros, B. Bougioukou, G. Giustini, Computational fluid dynamics prediction of subcooled boiling of water using a mechanistic bubble-departure model, Nucl. Eng. Des. 412 (2023) 112465.

[12] J.R.S. Thom, W.M. Walker, T.A. Fallon, G.F.S. Reising, Boiling in sub-cooled water during flow up heated tubes or annuli, Proc. Inst. Mech. Eng. 180–3C (1965-66) 226–246.
[13] T.B. Nguyen, T. Okawa, Experimental validation of the mechanism and condition for the onset of significant void in subcooled flow boiling, Int. J. Heat Mass Tran. 219 (2024) 124881.
[14] S. Dong, T. Hibiki, Evaluation of models and correlations for onset of significant void in subcooled boiling flows in channels with various geometries, Int. J. Heat Mass Tran. 245 (2025) 127028.
[15] G.G. Bartolomei, V.N. Mikhailov, Enthalpy of the start of intensive vapor generation, Therm. Eng. 34 (1987) 67–70.
[16] T. Hibiki, One-dimensional drift-flux correlations for two-phase flow in medium-size channels, Exp. Comput. Multiphas. Flow 1 (2019) 85–100.
[17] T. Hibiki, C. Dong, N. Tsukamoto, Full-range drift-flux correlation for upward co-current two-phase flows in vertical pipes, Int. J. Energy Res. 2025 (2025) 6193526.
[18] T. Hibiki, N. Tsukamoto, Drift-flux model for upward dispersed two-phase flows in a vertical rod bundle, Appl. Therm. Eng. 226 (2023) 120323.
[19] T. Hibiki, S. Dong, Modeling axial void fraction profile of upward subcooled boiling flows in vertical round tubes, Appl. Therm. Eng. 280 (2025) 128309.
[20] G.G. Bartolomei, V.G. Brantov, YuS. Molochnikov, YuV. Kharitonov, V.A. Solodkii, G.N. Batashova, V.N. Mikhailov, An experimental investigation of true volumetric vapor content with subcooled boiling in tubes, Therm. Eng. 29 (1982) 20–22.
[21] P.G. Kroeger, N. Zuber, An analysis of the effects of various parameters on the average void fractions in subcooled boiling, Int. J. Heat Mass Tran. 11 (1968) 211–233.
[22] F.J. Collado, C. Monne, A. Pascau, D. Fuster, A. Medrano, Thermodynamics of void fraction in saturated flow boiling, J. Heat Tran. 128 (2006) 611–615.
[23] F.J. Collado, C. Monne, A. Pascau, A new heat balance for flow boiling, AIChE J. 53 (2007) 2123–2130.
[24] Z. Bilicki, E.E. Michaelides, Thermodynamic non-equilibrium in liquid-vapor flows, J. Non-Eq. Thermo. 22 (1997) 99–109.
[25] G.A. Knights, A Study of Two-phase Pressure Drop and Density Determination in a High-Pressure steam-water Circuit, Cambridge University Engineering Laboratory, Cambridge, UK, 1960. Ph.D. Thesis.
[26] F.J. Collado, Reynolds transport theorem for a two-phase flow, App, Phys. Lett. 90 (2007) 024101.
[27] F.J. Collado, Void fraction thermo-kinematics for subcooled flow boiling, Phys. Fluids 34 (2022) 123302.
[28] R. Aris, Vectors, Tensors, and the Basic Equations of Fluid Mechanics, Dover Publ., Mineola, USA, 1990. Chap. 4.
[29] P. Griffith, J.A. Clark, W.M. Rohsenow, Void volumes in subcooled boiling systems, New York, USA, in: Proceedings of ASME Conference, 1958. Paper 58-HT-19.
[30] F-chart software. Available online: EES: Engineering Equation Solver | F-Chart Software : Engineering Software (accessed on February 19, 2026).
[31] J.M. Delhaye, F. Maugin, J.M. Ochterbeck, Void fraction predictions in forced convective subcooled boiling of water between 10 and 18 MPa, International Journal of Heat and Mass Transfer 47 (19-20) (2004) 4415–4425, https://doi.org/10.1016/j.ijheatmasstransfer.2004.05.018. https://linkinghub.elsevier.com/retrieve/pii/S0017931004002005.
[32] F.P. Incropera, D.P. De Witt, Fundamentals of Heat and Mass Transfer, third ed, Wiley, New York, USA, 1990. Chap. 8.